Non-destructive Optical Measurement of Transparent Objects: A Review

Hongda Quan, Wenqi Shi, Lingbao Kong*

Cite this article as: Hongda Quan, *et.al*. Non-destructive Optical Measurement of Transparent Objects: A Review. *Light: Advanced Manufacturing* accepted article preview 19 February 2025; doi: 10.37188/lam.2025.022

Received 2 April 2024; Revised 14 February 2025; Accepted 18 February 2025; Accepted article preview online 19 February 2025

Non-destructive Optical Measurement of Transparent Objects: A Review

Hongda Quan, Wenqi Shi, Lingbao Kong*

Shanghai Engineering Research Center of Ultra-Precision Optical Manufacturing, School of Information Science and Technology, Fudan University, Shanghai 200433, China

*lkong@fudan.edu.cn

Abstract

Transparent objects are widely used in various fields, leading to increasing demand for methods of measuring them. However, the measurement of such objects has always been challenging owing to the intricate refraction and reflection phenomena they exhibit. Given that traditional contact measurement methods can damage transparent objects, the use of non-destructive measurement techniques, particularly those based on optical principles, is considered preferable. As a result, various non-destructive measurement methods have been developed for transparent objects by leveraging the unique characteristics of light, and a comprehensive review is imperative for exploring these innovative methods and their potential applications. This review accordingly begins by elucidating the necessity of measuring transparent objects and exploring the concept of transparency. Next, an overview of various non-destructive optical measurement techniques spanning macro-, micro-, and general-scale applications is presented, followed by a discussion of their respective advantages and limitations. Finally, the paper concludes by outlining future directions for potential advancements in the field. This review is expected to serve as a valuable resource for newcomers in the field of transparent object measurement and assist researchers seeking to integrate these techniques into interdisciplinary studies.

Keywords: Transparent objects, Non-destructive measurement, Optical measurements

Introduction

Transparent substances are widely encountered in various aspects of life and include water[1, 2], cell cytoplasm[3], and the atmosphere[4]. Furthermore, transparent materials such as glass[5] and plastics[6, 7] are commonly utilised in industry. For example, the production of thin films[8] and displays[9] relies heavily on transparent materials. In addition, transparent materials play crucial roles in optics, where they are applied as lenses, prisms, and other instrument components[10].

The quality of a transparent object significantly affects its performance in application. Indeed, optical defects and faulty elements can negatively affect the required optical path or image quality and even damage other components[11-13]. Thus, the effective measurement of transparent objects is crucial for ensuring the desired quality and functionality. Contact measurement methods[14, 15] commonly employ a profiler, but may have limited accuracy owing to the required probe size. Though atomic force microscopy can be employed to obtain more detailed measurements, this method can scratch the object surface, introducing secondary errors and damage. As a result, the use of non-destructive measurement methods that do not damage the measured object is preferred. Optical measurement is considered an ideal non-destructive approach, although the complex optical properties of transparent objects make such measurements challenging. As defining the measurement target is the first step in determining the appropriate measurement method, the meaning of "transparent" must be defined.

Definition and Relativity of Transparency

Transparency is typically determined by the balance between the directly transmitted and scattered light passing through a medium, which are respectively measured in terms of transmittance and haze[16-18]. Transmitted light conveys information indicative of clarity and transparency, whereas scattered light degrades quality, resulting in haze. Consequently, defining transparency using a single numerical standard is challenging, as each application scenario has its own criteria for

"transparency". For example, the transmittance rate that defines "transparency" for transparent heaters is greater than 90%[19], whereas that for transparent solar cells and organic photovoltaics[20, 21] is typically approximately 20% and that for transparent paper[22] is approximately 60%. Typically, an object is considered transparent if the transmitted light accounts for more than 50% of the incident light in most application scenarios[23, 24]. The concept of transparency typically discussed in relation to measurement applications refers to situations in which the signal-to-noise ratio of the reflected or scattered light passing through the object is relatively low, rendering conventional measurement methods ineffective and necessitating the development of new techniques for measuring transparent objects.

Transparency is also relative to the specific wavelength range considered. Indeed, the Fresnel equations indicate that transmittance and reflectance are related not only to the incidence angle but also to the refractive index (RI) of the medium, and the RI is wavelength dependent, as described by the Lorentz dispersion model and defined by the Helmholtz equation:

$$n^2 = 1 + \sum_j \frac{b_j \lambda^2}{\left(\lambda^2 - \lambda_j^2\right) + g_j \lambda^2 / \left(\lambda^2 - \lambda_j^2\right)} \quad (1)$$

where b_j, g_j, λ_j, and j are constants determined by the medium itself. As a result, the transmittance of a medium does not only depend on its own properties but also the wavelength of the incident light.

In summary, transparency is difficult to quantify using a single numerical value such as transmittance and must be interpreted within the context of each specific application. This review considers transparent objects to be those in which the transmitted light exceeds the absorbed or scattered light, rendering conventional measurement methods ineffective, and is focused on methods for measuring such objects accordingly. Moreover, as transparency is a wavelength-dependent concept, this review focuses on methods for measuring objects that are transparent within the visible-light range (400–700nm), which are more common and have greater research significance. However,

techniques that are suitable for measuring objects transparent to visible light can often be adapted to inspect objects transparent to other wavelengths.

Refraction and Reflection in Transparent Objects

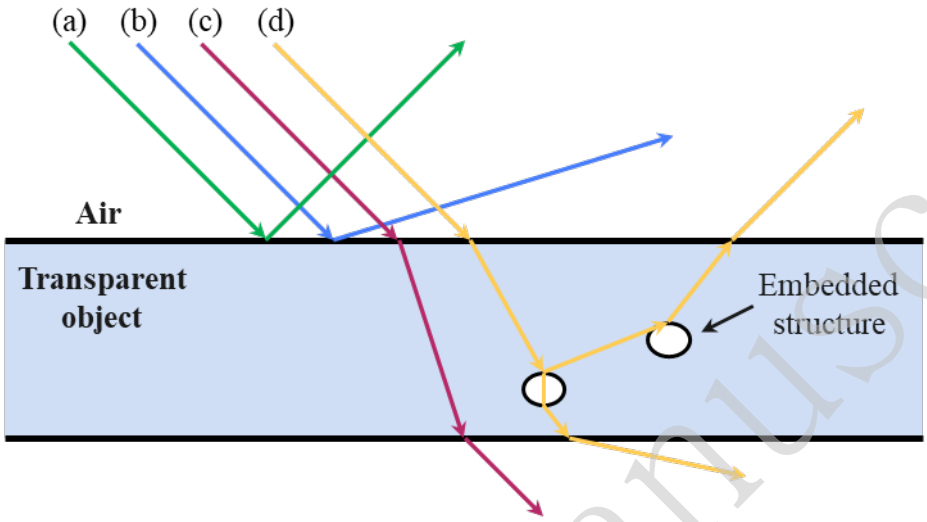

Figure 1. Complex refraction and reflection phenomenon in transparent objects. Lines (a)–(d) denote specular reflected light, scattered light, transmitted light, and complex refracted and reflected light interacting with embedded structures, respectively.

Transparent objects pose a significant challenge for optical detection because of their associated complex refraction and reflection phenomena. Typically, transparent objects are observed in air, where the incident light encounters several situations simultaneously, as illustrated in Fig. 1:

(a) specular reflection, which occurs when the incident light is directly reflected

(b) direct scattering

(c) refraction inside the object as the light passes through

(d) refraction and interaction with structures embedded within the object, which result in complex reflected and refracted light that is often of low intensity.

Thus, the effective measurement of transparent objects necessitates capturing refracted or reflected light. The modulation and influence of a transparent object on incident light can be understood by analysing the changes in light intensity, phase,

polarisation, and spatial angle. Such analyses provide detailed information describing the surface morphology, internal structure, and RI distribution of the observed transparent object, enabling quantitative measurements.

Because measurement techniques and methods are often closely related to the scale of measurement, this review categorises measurement methods based on their deployment on macro-, micro-, and general scales, as shown in Fig. 2. The specific requirements for different measurement targets are also discussed to address the relationship between the scale and measurement method and compare the advantages and limitations of each method. Finally, the review concludes with a summary of potential improvements to these methods.

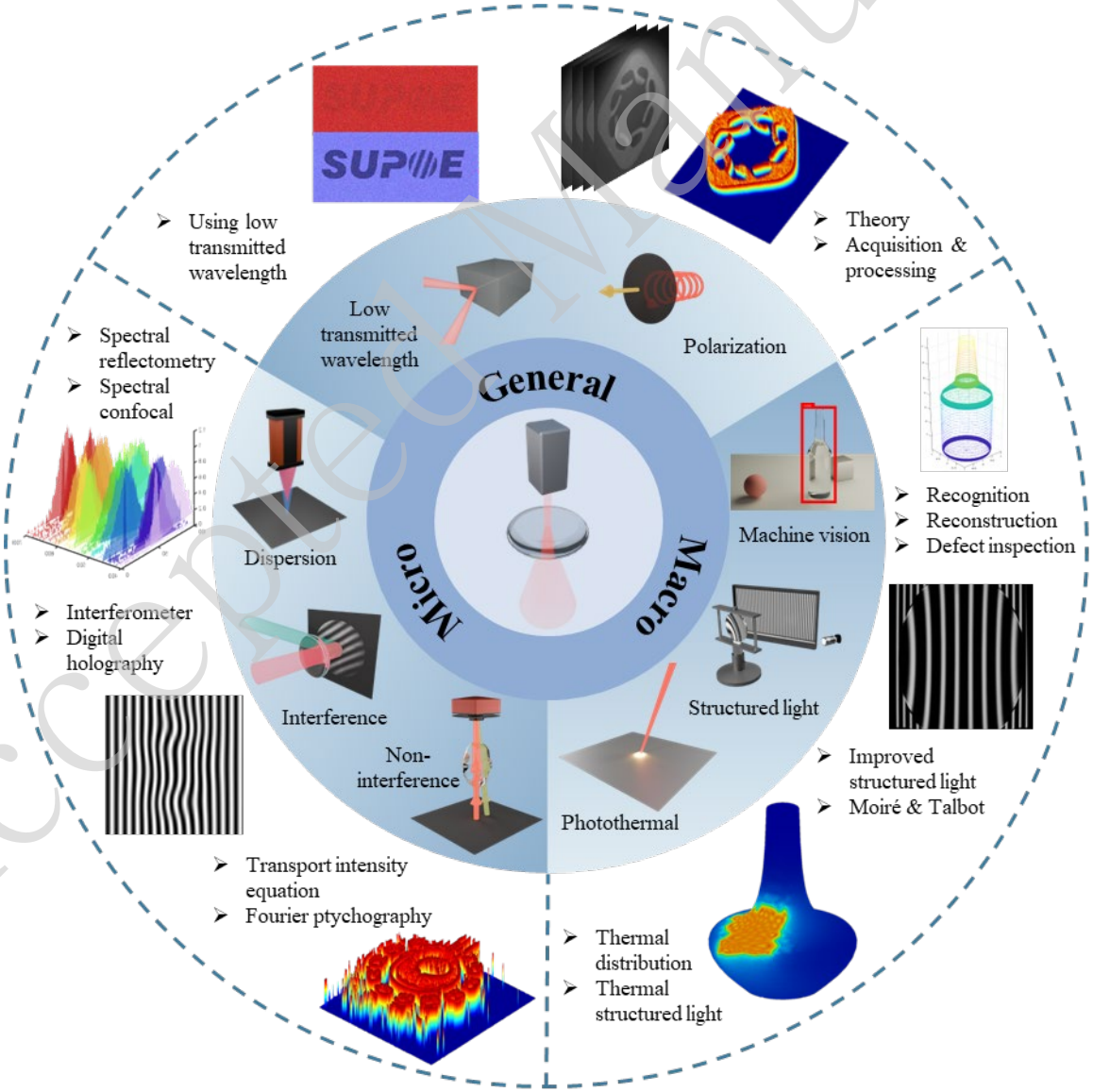

Figure 2. Overview of non-destructive optical measurement methods for transparent objects.

Macro-scale Measurement Methods

This section discusses optical measurement methods for macro-scale objects, which typically range in size from centimetres to millimetres and even microns. Macro-scale transparent object measurement plays a significant role in various applications, including autonomous driving and industrial robotics. For example, the accurate identification of transparent objects such as glass walls is essential for the safe operation of autonomous vehicle, assisted vision, and automatic navigation systems; distinguishing between glass and plastic containers is a vital task for laboratory automation; transparent object recognition is crucial for waste sorting and item classification; and precise reconstruction and defect detection are critical in industrial contexts such as the manufacture of glass display substrates.

The key challenge associated with obtaining macro-scale measurements is to achieve both speed and accuracy. The following sections accordingly discuss machine vision methods according to application, then conventional and improved structured light techniques before exploring innovative approaches that utilise photothermal principles.

Machine Vision Methods

The increasing demand for higher accuracy and efficiency in workpiece inspection has led to the widespread use of machine vision methods. These methods typically capture images using charge-coupled devices or complementary metal oxide semiconductor sensors, then conduct image analyses to extract the geometric dimensions, defects, and other relevant information describing the object being measured. Different system architectures have been employed according to the specific measurement target. This section focuses on transparent object recognition and segmentation as well as reconstruction. Defect detection, which is critical in industrial manufacturing, is discussed separately because of its special identification requirements.

Transparent Object Recognition and Segmentation

There is a considerable demand for transparent object recognition and segmentation in the robotics and autonomous vehicle fields. Segmentation and recognition problems typically require the identification of object features. In 2005, McHenry et al. proposed a transparent object feature recognition method that utilises the distortion along the edges of the transparent object and the inherent highlighting phenomenon on its surface to realise segmentation[25]; however, this approach is limited by the environmental conditions in which it is employed. Researchers have proposed recognition and segmentation methods that capture additional types of information to address this limitation. In 2015, Xu et al. proposed a light-field distortion feature[26] that provides a new model for the visual recognition of transparent objects, as shown in Fig. 3. This method was subsequently applied to realise the segmentation of transparent objects[27]. In addition to using light-field information to improve segmentation results[28-30], depth information has also been applied. Missing depth information has been integrated into a Markov random field to segment transparent objects[31] with improved results. Indeed, various methods for describing the transparent object features extracted from the light field and depth information have been proposed to enable effective recognition and segmentation.

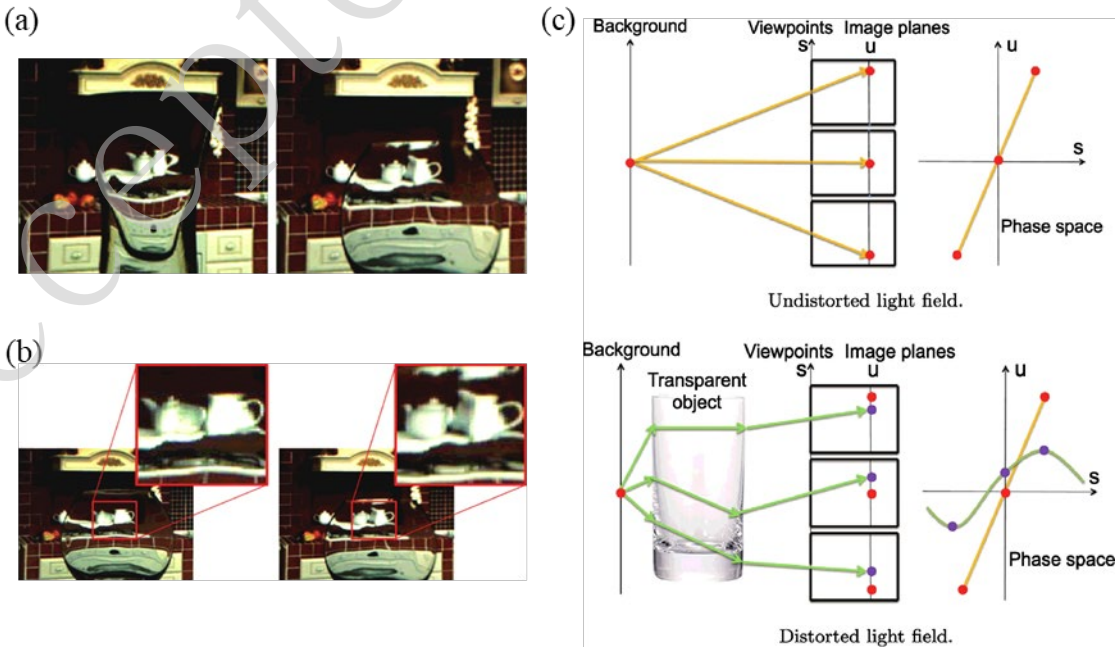

Figure 3. Light field distortion feature for transparent object recognition and segmentation Reproduced with permission[26]. Copyright 2015, Elsevier Inc. (a) Background distortion from different objects and **(b)** background distortion from changing viewpoints, showing that the distortion of the light field is closely related to the object itself. **(c)** Light field propagation, showing that the involvement of the transparent object changes the distribution and phase of the light field.

Rapid advances in computer science have contributed to the development of valuable technologies such as deep learning and their application to transparent object measurement. Indeed, remarkable progress has been made recently in image-segmentation techniques using deep learning with widespread applications across various fields. Madessa et al. proposed the mask region convolutional neural network to detect a single transparent object[32]; Xu et al. used the dense connections between different atrous convolution blocks to restore more detailed information[33]; and Yu et al. designed the discriminability enhancement and focus-and-exploration-based fusion modules to implement coarse-to-fine glass segmentation[34]. Various neural networks have also been proposed to perform transparent object segmentation tasks[35-37].

However, these approaches generally exhibit poor accuracy, making them suitable for approximate estimation only. Thus, the combination of machine vision-related algorithms with high-precision measurement approaches represents a promising direction for future research.

Transparent Object Reconstruction

Reconstruction is a crucial task in measurement, and is typically based on triangulation principles. Kutulakos and Steger elaborated on light triangulation measurement theory to discuss single-view specular depth estimation and three-view double refractive–reflective reconstruction[38]. They noted that reconstructing objects more than three times by increasing the view-angle refraction was impossible.

Other methods approach transparent object measurements from alternative perspectives. Kim used an algorithm based on highly asymmetrical prior conditions to reconstruct the inner and outer surfaces of transparent objects[39], and Koyama et al. employed ultraviolet (UV) light using a structure-from-shading (SfS) method to reconstruct transparent objects[40], as shown in Fig. 4(a)-(b). In addition, backpropagation

has been applied to infer the scattering parameters of transparent objects: Gkioulekas et al. proposed using backpropagation to infer the distribution of the internal scattering parameters of a semi-transparent object[41], as shown in Fig. 4(c), and Che et al. suggested using backpropagation to measure the distribution of internal secondary scattering by combining the stochastic gradient descent and Monte Carlo simulation, offering a new approach for measuring transparent material parameters[42].

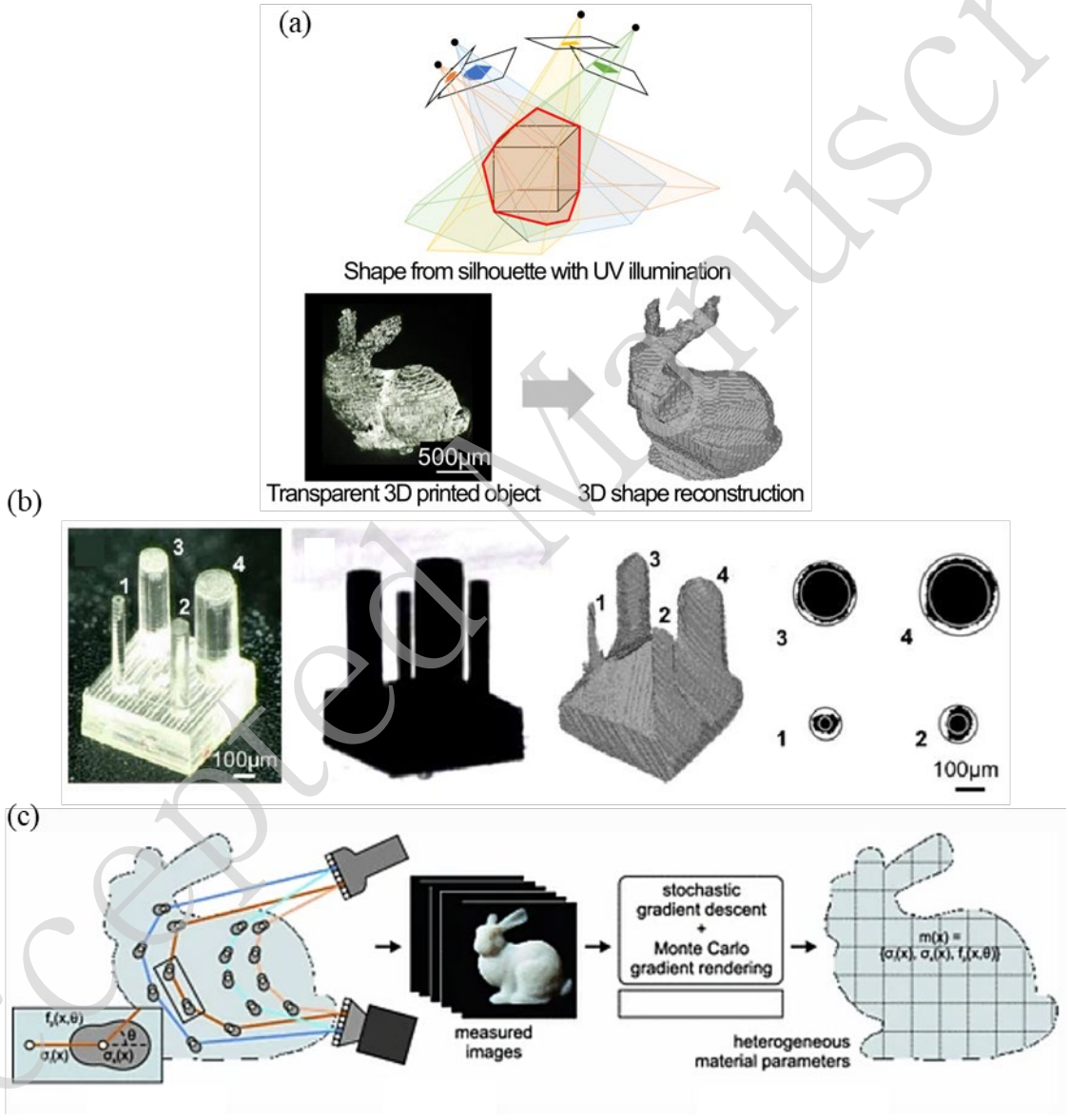

Figure 4. **(a)** Overview and **(b)** results of the SfS method using UV, showing, from left to right, the optical microscope image, silhouette obtained using UV illumination, reconstruction of the pillar array model using the SfS method, and a cross section at half height of each reconstructed pillar. Reproduced with permission[40]. Copyright 2018, CC BY 4.0. **(c)** Inverse scattering model used to measure the scattering parameters inside a semi-transparent object by combining the

stochastic gradient descent and Monte Carlo simulation methods. Reproduced with permission[41]. Copyright 2016, Springer International Publishing AG.

Defect Inspection

The defect inspection of transparent objects requires specialised forms of recognition that can significantly enhance efficiency. Various defect detection methods have been combined with different image processing algorithms to considerably improve inspection efficiency and reduce inspection costs in manufacturing applications[43-45]. For example, Gong et al. achieved a defect detection accuracy of 99.5% at an inspection speed of 60 bottles/min for over 60,000 bottles using custom-made blue dome illumination with deformable template matching and an adaptive threshold selection strategy[46]. Deng et al. demonstrated a method for measuring embedded microstructures in transparent objects that treats defects as microlenses to determine their depths by analysing the differences in the grayscale values of their transmitted light[47, 48].

The integration of machine learning has introduced new solutions for the defect inspection of transparent objects. Erozan et al. introduced a learning-based optical inspection method for transparent printed electronics that achieved a 95% defective transistor detection rate[49]. Yin et al. combined the machine vision and machine learning methods illustrated in Fig. 5 to inspect large-aperture optics with a minimum detectable flaw size of 20 microns and a flaw position accuracy of better than 50 microns[50], demonstrating the potential of applying machine learning in the defect inspection of transparent objects. Furthermore, the efficiency and accuracy of film inspection have also been improved using machine learning[51]. Indeed, the active application of machine learning in defect detection methods represents a promising research direction.

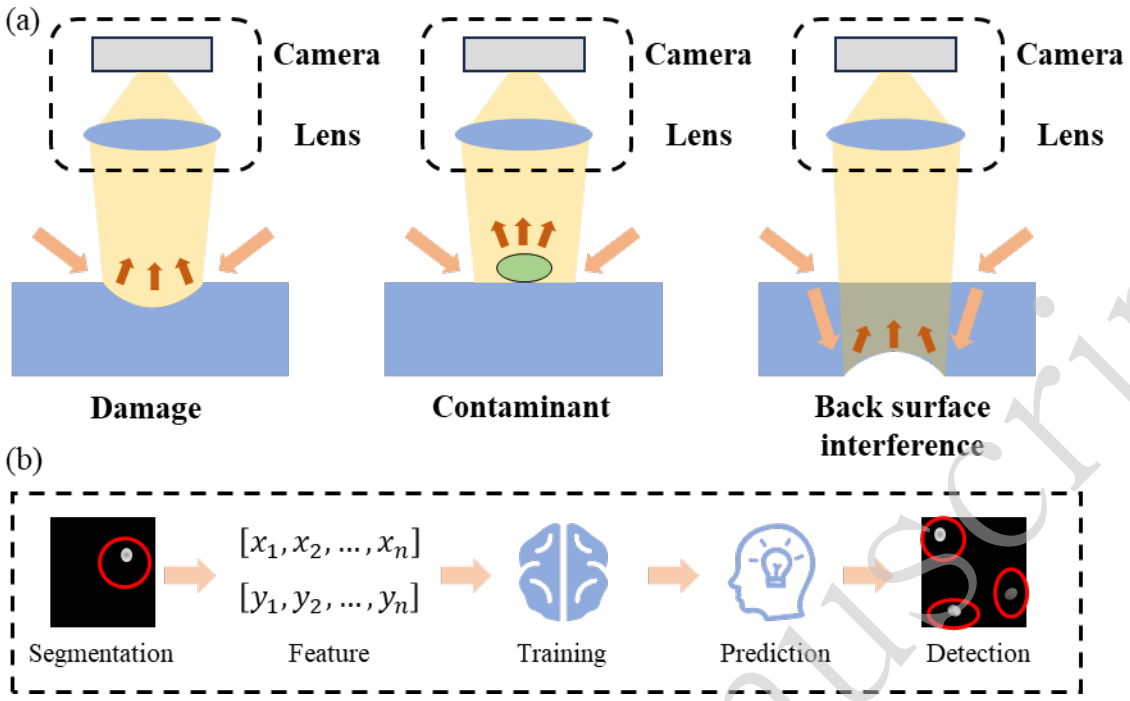

Figure 5. Efficient and precise detection of surface flaws based on machine vision and machine learning. (a) Flaw detection using the dark-field method, showing, from left to right, damage, contaminant, and back surface interference. **(b)** Framework of the surface flaw inspection algorithm.

Edge enhancement is a commonly used technique for defect detection, and recent advancements in metasurface technology have enhanced this technique using metasurface-based differential interference contrast (DIC). Indeed, the development of metasurfaces capable of light-field calculations has expanded the human ability to manipulate light[52-58]. In contrast to the Wollaston prism, metasurfaces can perform differential operations to extract object edges, significantly improving upon DIC performance[59-62]. However, the manufacture of metasurfaces remains challenging, and further work is required to improve associated quantitative measurement techniques.

Structured Light Methods

Structured light is a measurement technology derived from machine vision that was primarily developed to address pixel ambiguity in general applications. Current applications of structured light include fringe projection profilometry (FPP)[63-66] for diffuse reflective objects and phase measurement deflectometry (PMD)[67] for highly reflective objects, as illustrated in Fig. 6. These mature methods can efficiently reconstruct object shapes based on the distortion of stripes by the surface of the

observed object.

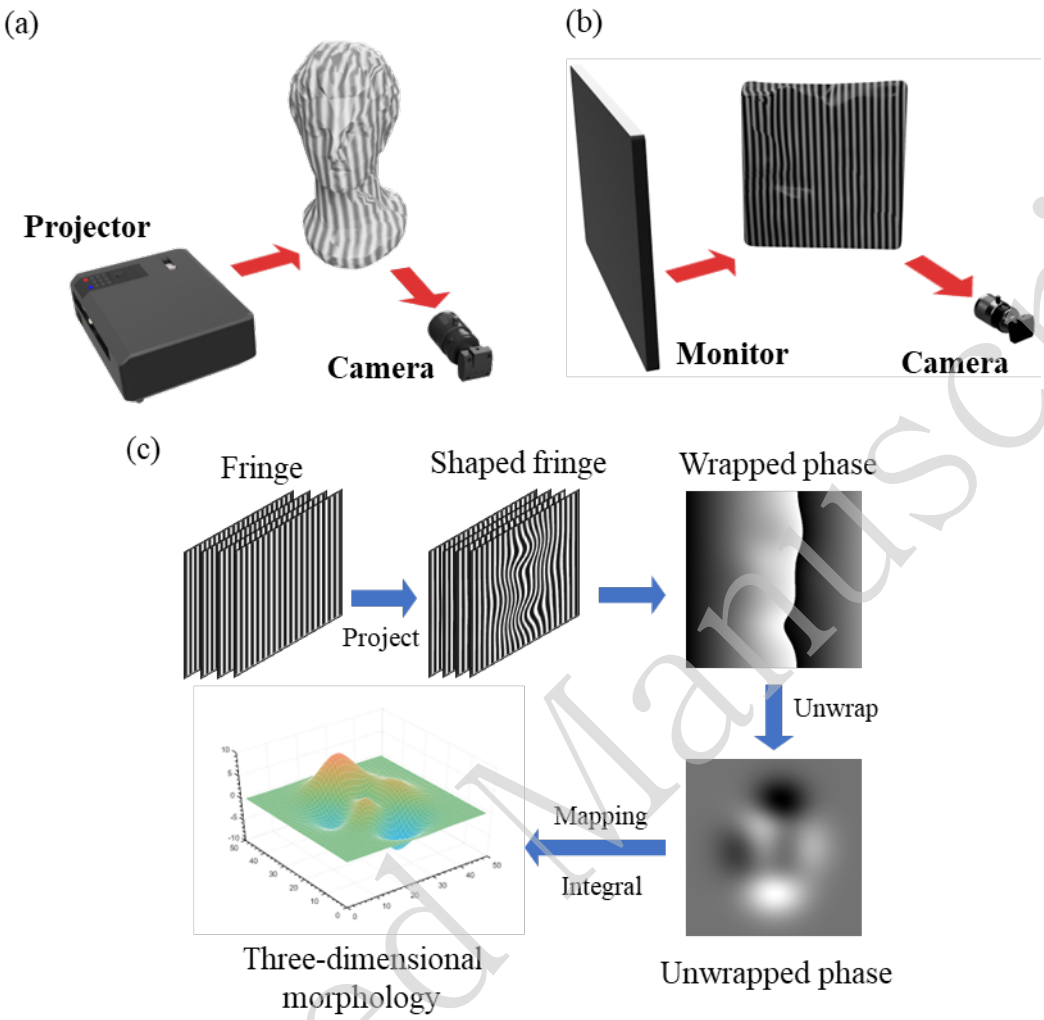

Figure 6. Schematic diagram of FPP and PMD. (a) Structure of the FPP system, including projector and camera. The projector projects a fringe onto the observed object that is modulated by the object and captured by the camera. **(b)** Structure of the PMD system, including monitor and camera. The monitor displays the fringes reflected and modulated by the highly reflective object being measured. **(c)** Flowchart for reconstruction using structured light. First, phase-shifted sinusoidal fringes are generated and projected onto the measured object to capture deformed fringe patterns. The wrapped phase map is subsequently extracted from these deformed images, then phase unwrapping is conducted to produce the absolute phase map. Finally, this map is utilised to reconstruct the three-dimensional morphology of the object. Notably, after calibration, the absolute phase in FPP can be directly correlated with the actual height of the object, whereas in PMD, the absolute phase corresponds to the gradient and requires integration to recover the true object shape.

However, both FPP and PMD face challenges when inspecting transparent objects owing to the presence of weakly reflected light, which results in lower-quality fringes and poorer reconstruction results. Researchers attempting to overcome this problem

have proposed improvements and optimisations from various perspectives, as discussed in the next section.

Improved Structured Light

Attempts to optimise the structured light method for the measurement of diffuse and highly reflective objects have been widespread. One approach for doing so is to enhance traditional structured light systems using multi-sensor fusion. For example, Ji et al. combined red–green–blue (RGB) images with structured light data to fill in missing parts in the observation of the transparent object and reported improved measurement results[68], as shown in Fig. 7(a). However, this method may not fundamentally improve the reconstruction accuracy. Another approach involves changing the structured light coding method to separate the secondary reflected light. Lei et al. achieved this by projecting two different frequencies of fringe-structured light[69], whereas Ye et al. decoupled the coupled fringes formed by the light reflected off of the upper and lower surfaces during PMD[70], enabling in situ measurements of transparent objects. Furthermore, Yang et al. proposed the novel encoding method illustrated in Fig. 7(b) to better address object highlights and transparency[71]. In addition to employing the spatial modulation of structured light, Liu et al. resolved the ambiguity of multiple refracted and reflected points in transparent objects by dividing the fringes in the time domain[72], and He et al. introduced the laser tracking frame-to-frame (LTFtF) method shown in Fig. 7(c)[73], which distinguishes the front and back surface reflections by comparing the moving speeds between neighbouring frames. The use of structured light methods with low-transmittance wavelengths, such as UV, can also be effective. Rantoson et al. used a binocular vision UV structured light system to measure transparent objects[74]. Moreover, Gu et al. combined structured light with compressed sensing to successfully measure and reconstruct transparent objects such as smoke, fog, and glass-embedded structures[75].

Another approach for improving structured light methods involves analysing the properties of the transmitted and scattered structured light using new theories. For example, Huang et al. analysed mathematical models of the transmitted and reflected

structured measurements collected from transparent objects[76], Guo et al. reconstructed the shape of a transparent object by leveraging the spatial frequency variation of the fringes[77], and Trivedi et al. utilised the Eikonal equation to derive the relationship between the transparent object and distorted transmitted structured light[78].

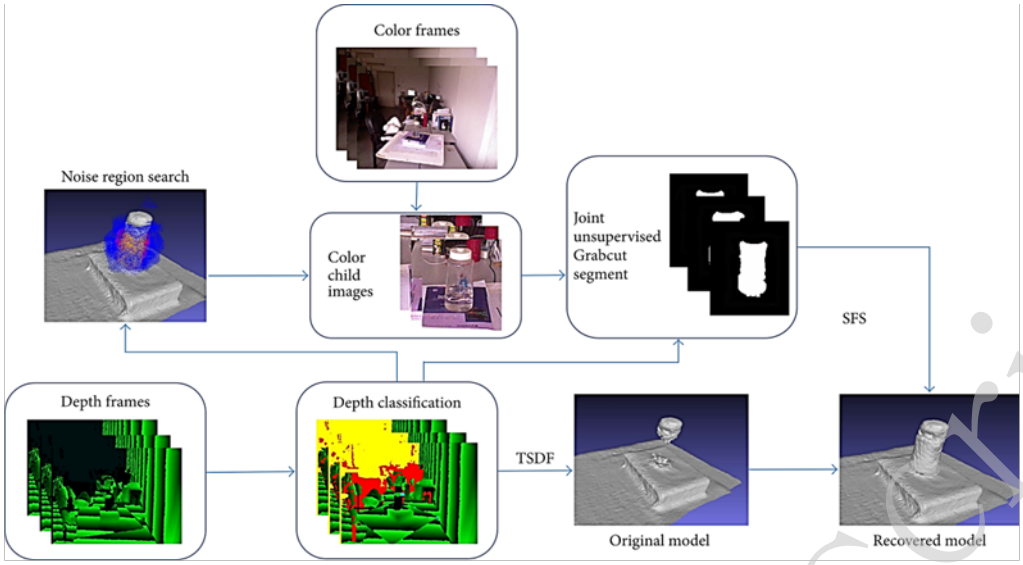

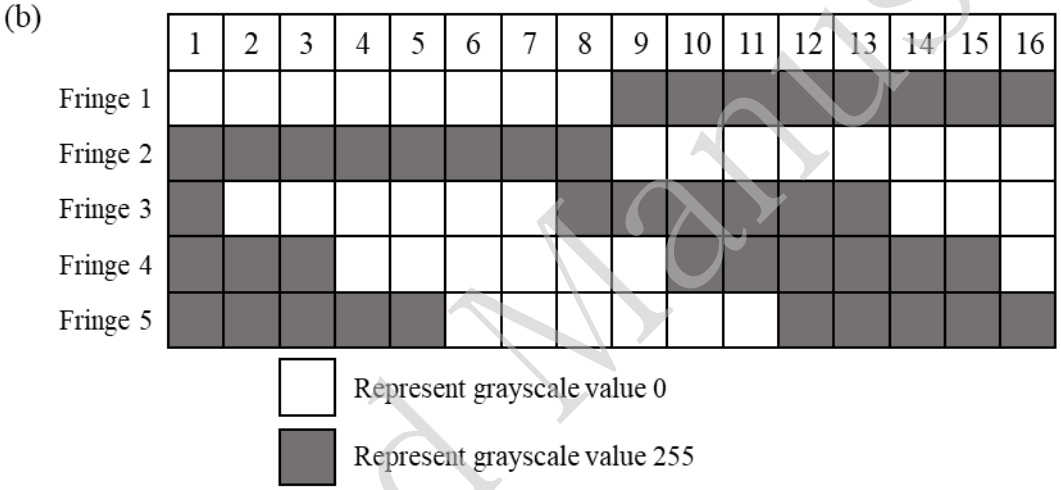

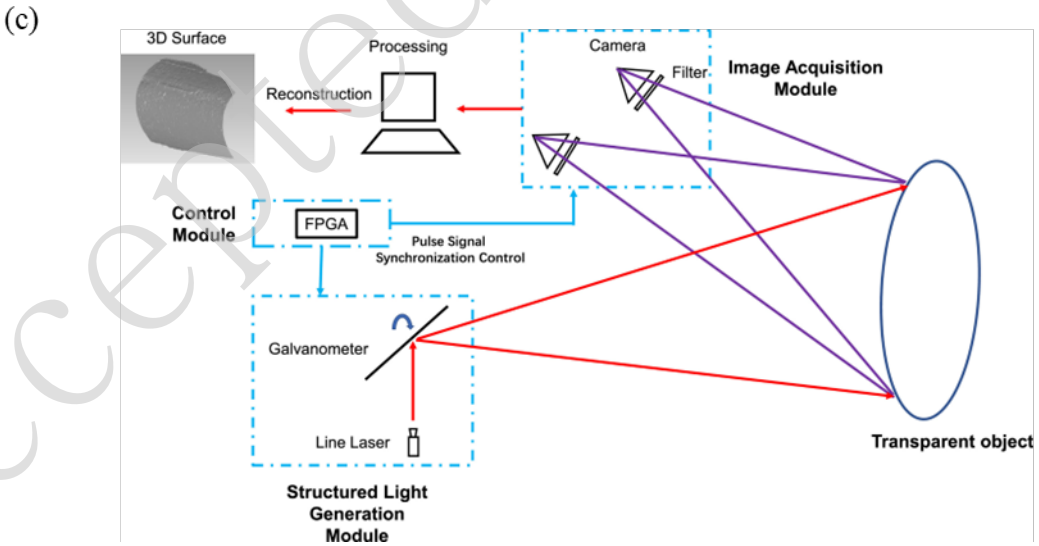

Figure 7. (a) Overview of method fusing RGB images with the depth data measured by the structured light framework. Reproduced with permission[68]. Copyright 2017, Creative Commons Attribution 4.0 International License. **(b)** A novel encoding method for structured light that overcomes highlights and transparency, in which five fringes are required in a single measurement

process. **(c)** System setup for the LTFtF method, which uses a line laser to scan and capture the reflected light with binocular vision. Reproduced with permission[73]. Copyright 2022, Elsevier Inc.

Moiré Patterns and the Talbot Effect

Moiré patterns[79] and the Talbot effect provide effective avenues for measuring transmitted structured light. As shown in Fig. 8(a), Xu and Liechti utilised moiré deflectometry to detect the focal length of transparent films[80] by adding the self-image of the transparent object to the grating and thereby generating moiré patterns, facilitating the measurement of light refraction. Similarly, Ri and Muramatsu used moiré patterns to measure the flatness of a glass plate[81] by utilising the misalignment of the grating image transmitted through the plate to measure its thickness. Thakur et al. measured transparent objects by inducing interference between the grating self-image modulated by the object and a reference grating, allowing the transparent object information to be inversely solved according to the interference fringes[82]. Meziane et al. utilised the grating image transmitted from a transparent object at an angle to a reference grating to form a moiré pattern, as shown in Fig. 8(b)[83]. A combination of the Talbot effect and Moiré pattern can also be used to measure the RI of a transparent medium, as demonstrated by Bhattacharya[84]. Indeed, moiré patterns and the Talbot effect can complement each other, and when combined with modern structured illumination microscopy [85], they hold promise for the inspection of microstructures at scales ranging from millimeters to microns.

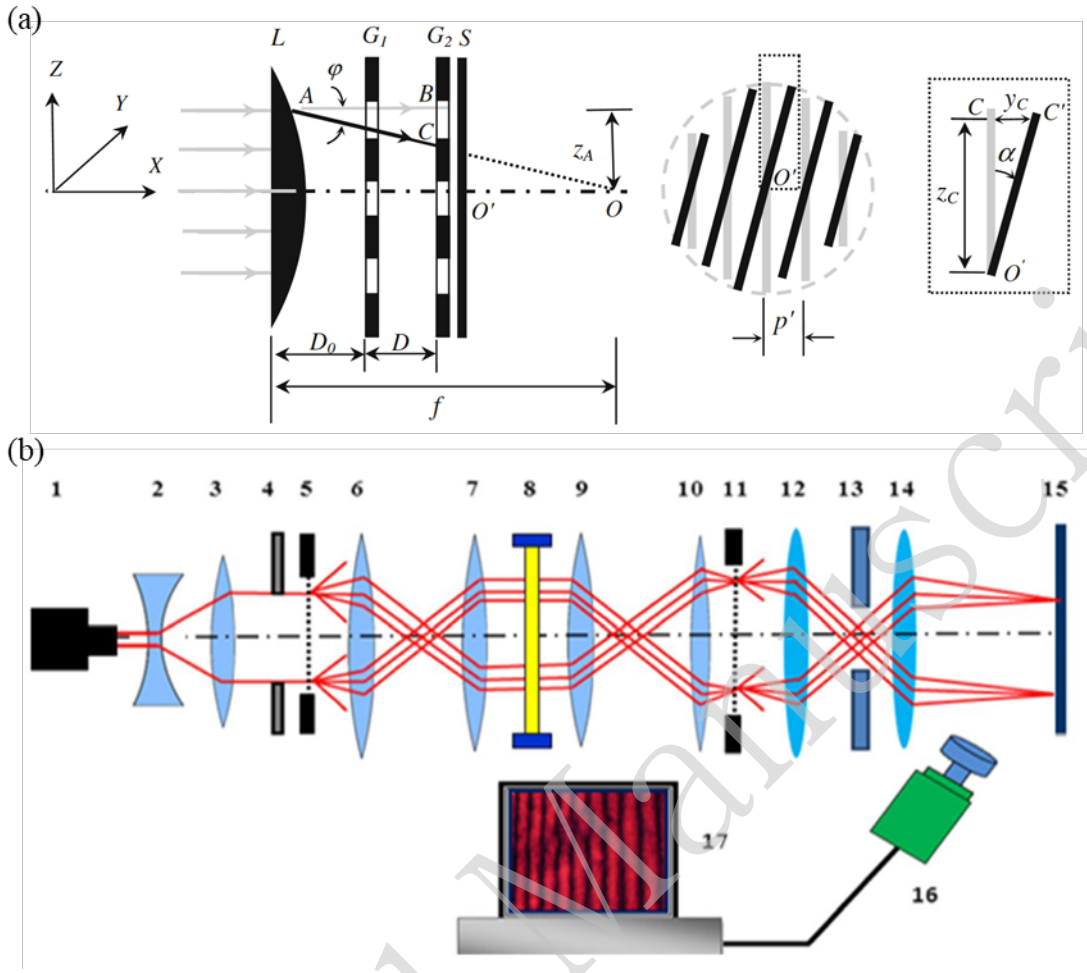

Figure 8. (a) Measuring the focus of transparent films using Moiré deflectometry, which relies upon the generation of a Moiré pattern by refracted light interacting with the reference grating. Reproduced with permission[80]. Copyright 2009, Society for Experimental Mechanics. **(b)** System setup for the measurement of transparent objects using the Talbot effect, in which 5 and 11 are gratings and 8 is the object under inspection. Reproduced with permission[83]. Copyright 2023, Springer-Verlag London Ltd., part of Springer Nature.

Photothermal Measurement Methods

Eren et al. proposed a novel method the optical measurement of transparent objects that comprises heating the object, then analysing its thermal distribution[86]; this represents an unconventional approach for optical measurement [87]. Meriaudeau et al. used laser scanning and an infrared camera to analyse the thermal distribution for object reconstruction[88], and Gong and Bansmer utilised a mid-infrared laser to scan ice and reconstruct the melting process[89]. Anika et al. projected thermal fringes using a carbon dioxide laser and reconstructed a transparent object using binocular infrared vision[90], and Landmann et al. used photothermal fringes to reconstruct the shapes of transparent

objects[91]. In contrast to the method employed by Anika et al., Landmann et al. proposed the encoding of structured light to minimise errors owing to thermal diffusion; these approaches are compared in Fig. 9. These studies suggest that photothermal methods hold promise for measuring transparent objects and overcoming the measurement difficulties associated with their unique optical characteristics.

However, photothermal methods have several limitations that can hinder their application: they cannot achieve completely non-destructive measurements because they may cause permanent damage to heat-sensitive materials, and they are more sensitive to environmental conditions because they rely on heat detection.

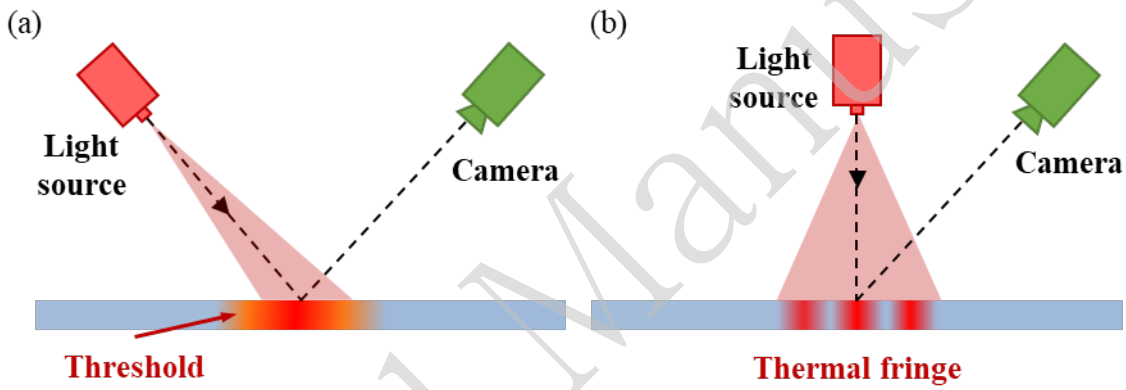

Figure 9. Two typical photothermal measurement methods. (a) Analysing the thermal distribution induced by a light source. **(b)** Analysing thermal structured light.

Micro-scale Measurement Methods

Micro-scale measurements, which are typically in the micron and even nanometre ranges, are crucial for assessing the microstructural quality of objects, especially in manufacturing applications, where issues such as substandard flatness or roughness can lead to overall component failure and hinder proper system functionality. Various methods have been developed for obtaining micro-scale measurements based on interference, non-interference, spectroscopy, and dispersion. Each approach offers unique capabilities for achieving accurate and reliable measurements at the micro-scale level.

Interference Methods

Interference represents a traditional approach for extracting the phase of light. The small scale of the wavelengths in the visible light range allows microscopic structures to be magnified into macroscopic phenomena such as interference fringes through the interference of light. Moreover, the advent of digital holography has brought new vitality and potential to interference-based methods by offering unique capabilities and opportunities for advanced applications.

Interferometry

Since its inception, interferometry has been instrumental in the high-precision measurement of microstructures. The underlying principle relies on the modulation of phase by the thickness of an object to represent phase differences using fringes through the interference between the object and reference lights. The introduction of the four-step phase-shift method revolutionised interferometry, enabling quantitative measurements. Subsequently, several modified schemes have been developed to address the limitations of traditional interferometry methods. This section focuses on methods used to generate interference fringes and obtain phase information through operations such as phase unwrapping.

Issues such as the secondary interference fringes produced by high-coherence light have been addressed through the introduction of the white-light interferometer utilising a low-coherence light source, as shown in Fig. 10. This approach has been applied to successfully measure transparent film layers: Petr summarised two methods for measuring transparent films using the white-light interferometer in 2004[92], and Sun et al. measured the thickness of transparent oil films on water surfaces using this technique in 2005[93]. Furthermore, Li et al. used white-light interferometry to measure the thicknesses, RIs, and dispersion constants of transparent films in 2012[94] and Audrey et al. combined white-light interferometry with tomography to detect defects in transparent polymers in 2015 [95]. Subsequently proposed methods have used white-light interferometry to effectively measure transparent films [96-100]. However, the limitations of interferometry when measuring thick transparent structures has restricted its widespread use.

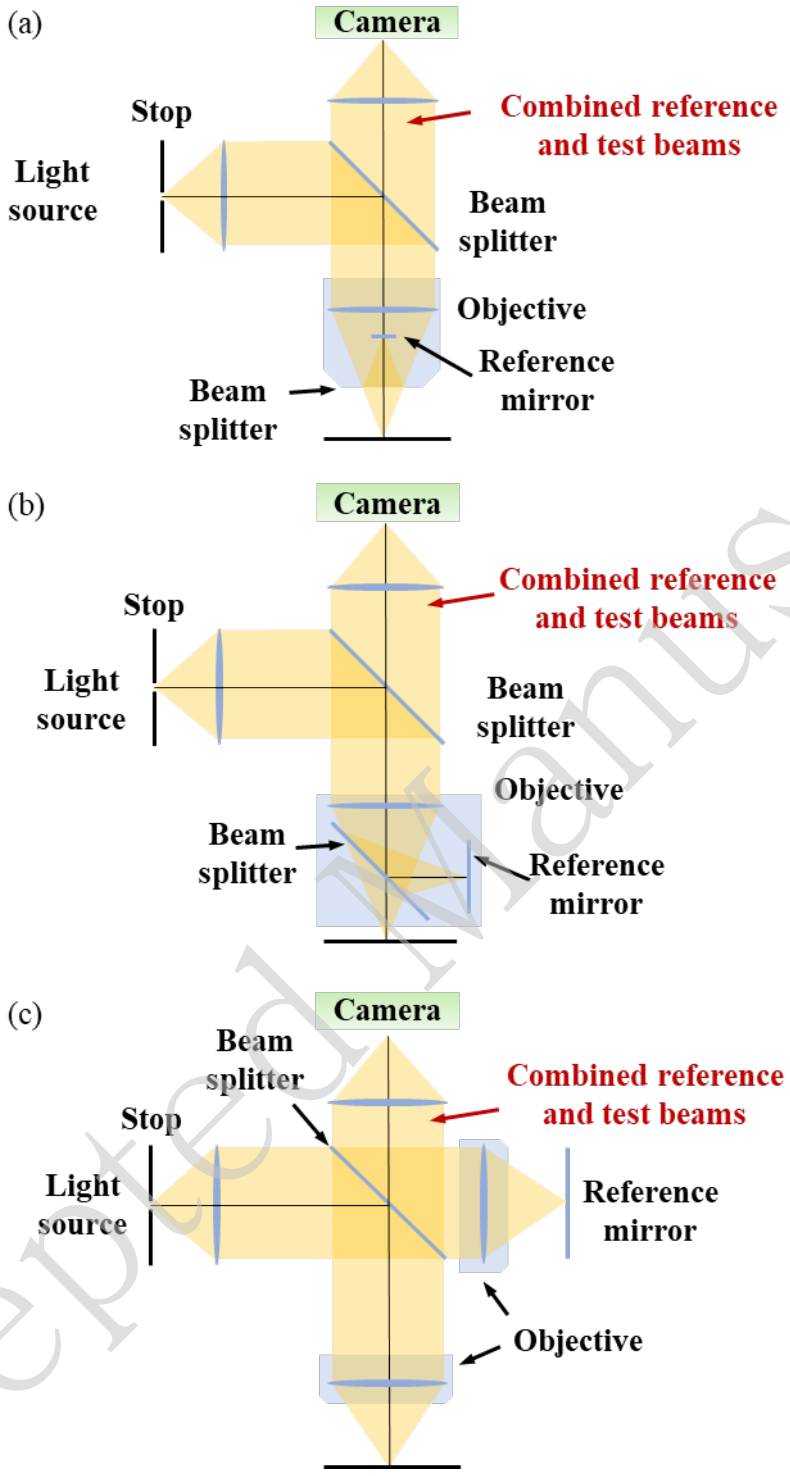

Figure 10. Three typical white-light interferometer setups. (a) The Mirau type, which is the most compact and provides excellent resistance to partial vibrations. **(b)** The Michelson type, which is suitable for low magnification, large field of view, long-working-distance objective lens designs. **(c)** The Linnik type, which is complex, but has an adjustable reference arm.

Digital Holography

Holography represents a special method of measuring objects using interference

fringes, and the development of digital holography[101-106] has particularly expanded the range of potential holography applications. Digital holography can be generally divided into on-axis or off-axis methods according to the structure of the optical path. A comparison of on- and off-axis methods is provided in Fig. 11. Each of these methods has different advantages in application.

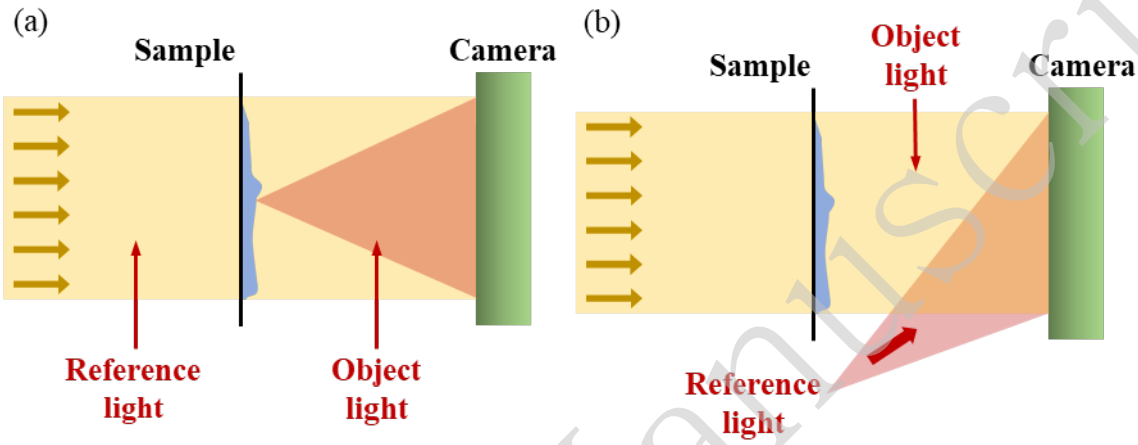

Figure 11. Two typical digital holography methods. (a) On-axis holography, in which the object light is scattered by the sample to transmit the reference light. **(b)** Off-axis holography, in which the reference light is directly transported to the camera to generate an interferometric fringe on the sensor.

Volker et al. elaborated on the principle of off-axis digital holography in 2001 and used it to measure microlens arrays[103]. Cuche et al.[107] and Kemper and von Bally[108] combined digital off-axis holography with phase-contrast techniques to obtain quantitative measurements of organisms. Techniques such as low-coherence light sources[109], multiple wavelengths[110-116], and multi-beam setups[117] have been employed to enhance the precision of and reduce the noise in digital holography measurements. Additionally, novel on-axis beam-splitting methods using prisms[118-120], diffraction gratings[121], plane mirrors[122, 123], and optical wedges[124] have been proposed to reduce the influence of environmental disturbances.

Indeed, interference fringes are highly sensitive to environmental disturbances, and even slight vibrations can lead to measurement failure. This issue is pronounced in the object–reference light interference methods above. As a result, object–object light interference[125] methods have been developed to significantly reduce the challenge of

obtaining reliable reference light. For example, in shear interferometry, the light phase information represents the thickness disparities between adjacent positions in the transparent object. Chhaniwal et al.[123] used parallel flat crystals to conduct transverse shear interferometry of tiny biological samples, leading to various derivative techniques[126-131]. Pinholes can also be used to obtain reference light, as demonstrated by Anand et al.[132] and Li et al.[133], who employed pinhole diffusers as shown in Fig. 12. Furthermore, Mahajan et al. employed a Sagnac interferometric structure with a special filter to generate reference light[134], whereas Jafarfard et al. combined this approach with dual wavelengths to realise improved accuracy[135].

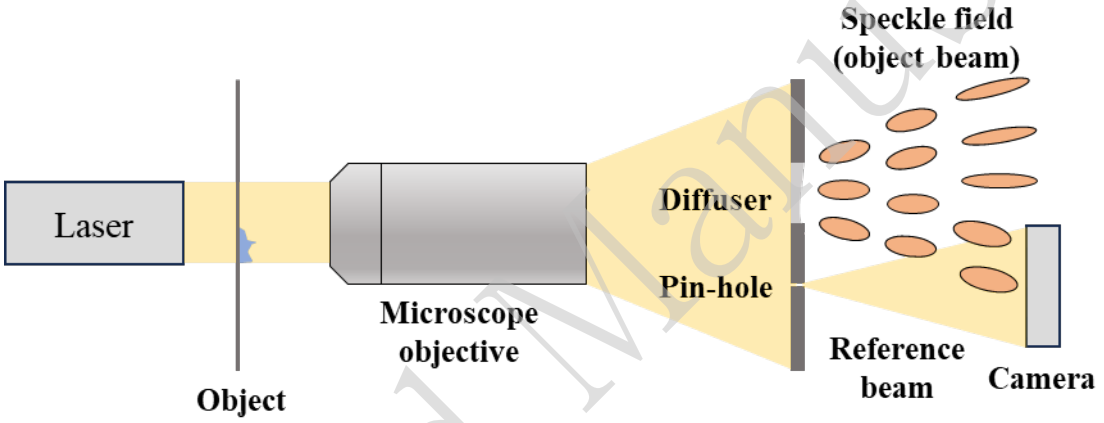

Figure 12. Quantitative phase microscopy based on single-beam Fourier transform digital holography. Experimental setup of single-beam lensless Fourier transform digital holographic microscopy. Reference beam, generated by pin-hole, interacts with object beam generated by diffuser to record phase information.

The post-processing of digital holography data has become a critical focus of research, resulting in the development of algorithms addressing the measurement speed[136], accuracy[137], and integration of sparse matrix solving and machine learning[138]. These advances have significantly enhanced the measurement capabilities of digital holography. Indeed, digital holography shows considerable promise for the measurement of transparent objects given their phase modulation properties, and continued advancements in algorithms and experimental setups are likely to achieve higher accuracy and speed in the future.

Non-interference Methods

Critically, interference methods suffer from serious drawbacks, such as high-coherence noise and stringent environmental requirements, that limit their widespread application. Consequently, novel methods and theories have been developed to overcome the constraints associated with conventional approaches for recording phase information using interference fringes. The observation of the light and dark stripes appearing at the bottom of a swimming pool in sunlight suggests that directly analysing the relationship between light phase and intensity represents a viable approach for doing so. Among the methods that circumvent the reliance on interference fringes using this approach, techniques based on the transport of intensity equation (TIE)[139] and Fourier ptychography[140], illustrated in Fig. 13, stand out as particularly promising.

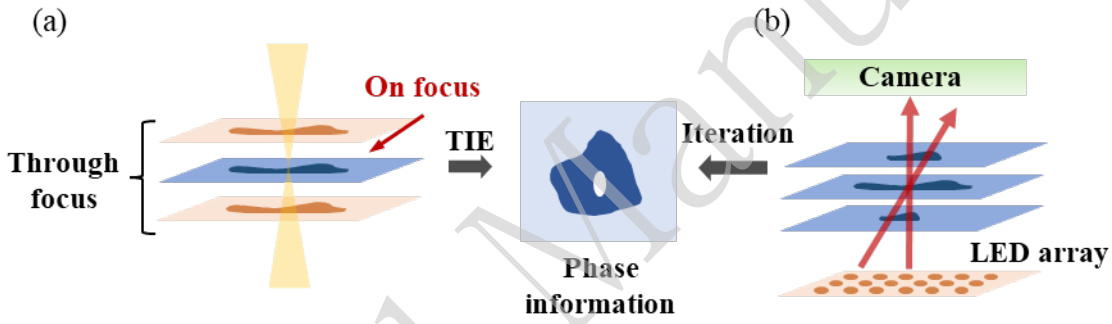

Figure 13. Schematic diagram of the principles underlying the TIE and Fourier ptychography methods. (a) The TIE method uses a through-focus image to calculate phase information. (b) The Fourier ptychography method uses different illumination angles to reconstruct phase information.

Transport Intensity Equation

The retrieval of phase information from intensity data began with the Gerchberg–Saxton (GS) phase iteration algorithm[141, 142], which was the first to enable quantitative phase measurements. This algorithm was improved upon by the Hybrid Input–Output algorithm proposed by Fienup[143]. Teague proposed the TIE in 1983[144]; this represents the first approach to obtain phase information numerically rather than iteratively. Zuo et al. later derived a generalised TIE based on the Wegner function that obeys the Liouville transport equation and is suitable for partially coherent illumination[145]. Barty et al. achieved phase tomography by rotating the sample[146], and Roberts et al.[147] and Ampem-Lassen et al.[148] used the TIE method to measure optical fibres. Kou et al.

combined the TIE with DIC microscopy[149] to improve the phase measurement results, Waller et al. utilised the information from multiple off-focus planes of intensity to enhance the accuracy of phase recovery and reduce noise[150], and Zuo et al. realised quantitative phase imaging of transparent living cells in real time using the TIE method[151, 152]. The TIE method has also been applied to the measurement of optical objects such as microlenses[153]. In 2015, Nguyen et al. obtained phase projections at various angles by rotating a transparent object and using the inverse Radon transform to reconstruct a three-dimensional model of it[154]. Since then, various schemes using the TIE to realise the three-dimensional reconstruction of objects have emerged, as shown in Fig. 14[155, 156].

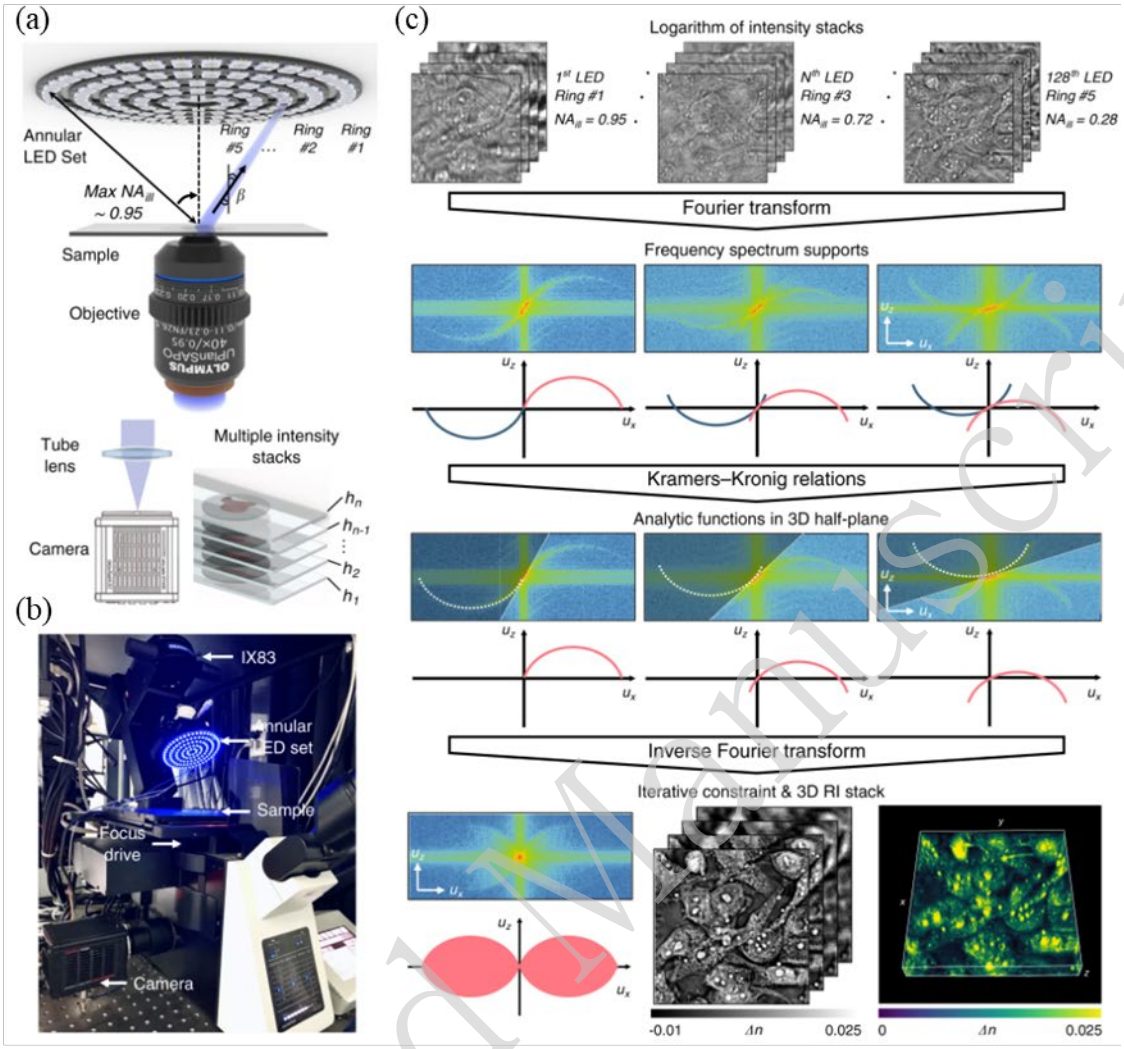

(d)

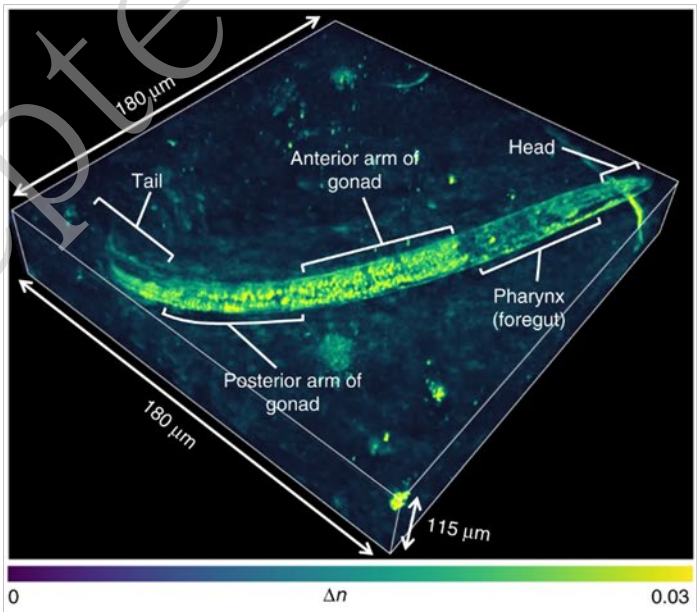

Figure 14. Three-dimensional reconstruction using transport of intensity diffraction tomography (TIDT). Reproduced with permission[156]. Copyright 2022, Creative Commons

 (a) Setup of TIDT system with a non-interferometric synthetic aperture (TIDT-NSA) based on a commercial microscope equipped with a multi-annular light-emitting diode (LED) array. **(b)** A photo of the system. **(c)** Flowchart of data processing in TIDT-NSA for three-dimensional RI reconstruction. **(d)** Three-dimensional RI rendering of *C. elegans* worm over a volume of $180 \times 180 \times 115$ μm.

Fourier Ptychography

In contrast to the TIE, Fourier ptychography[140] was initially proposed to address the need for high-resolution, large field-of-view imaging. Fourier ptychography essentially enables the tomography of transparent objects. In 2015, Li et al. utilised Fourier ptychography to achieve three-dimensional multilayer imaging[157]. Subsequently, the two mainstream methods described in Fig. 15 were developed: one that performs three-dimensional tomography through iteration in the Fourier spectral domain[158-159] and another that constructs a multi-slice model[160].

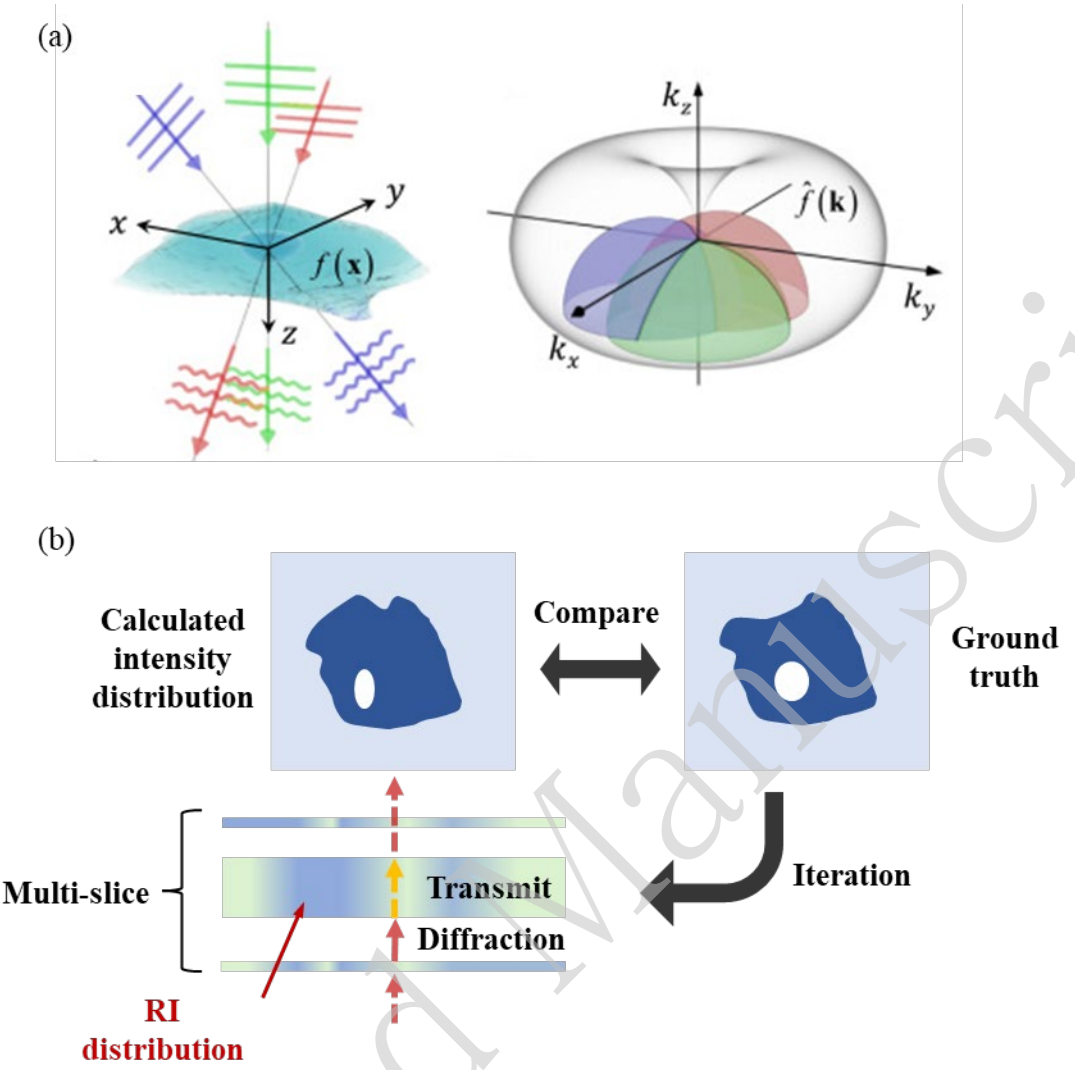

Figure 15. Typical Fourier ptychography methods for object reconstruction. (a) A three-dimensional sample is illuminated by plane waves from different directions, each generating a particular semi-spherical surface in the three-dimensional Fourier space. Reproduced with permission[158]. Copyright 2020, Creative Commons Attribution 4.0 International License. **(b)** Schematic of the multi-slice method, which sets the initial RI distribution randomly, then simulates the propagation of light to obtain the intensity distribution. The calculated intensity distribution is compared with the ground truth (captured by camera) to update the RI distribution; this process is iterated until the error between the two intensity distributions falls below the required limit.

Both the TIE and Fourier ptychography methods have shown significant potential for the measurement of transparent objects. However, the accuracy of quantitative phase measurements remains challenging. As a result, efforts to address issues such as the accurate calibration and control of measurement errors remain essential for applying these quantitative phase measurement methods in industrial applications.

Spectroscopy and Dispersion Methods

Spectroscopic measurement methods that utilise the different RIs of different wavelengths of light in the same medium, including the spectral reflectometry and spectral confocal methods, are commonly employed in thin-film inspection systems.

Spectral reflectometry is based on the principle that different wavelengths of light will experience enhancement or attenuation when passing through a film of a certain thickness with a specific RI owing to interference with the light reflected from its upper and lower surfaces. A combination of spectral reflectometry and ellipsometry has become the primary tool used for modern thin-film measurement[161-165], as illustrated in Fig. 16.

The spectral confocal method utilises a lens with significant dispersion to focus different wavelengths of light at different points, with only the light focused on the surface able to pass through the small holes in a conjugate position to be detected using a spectroscope. Thus, the thickness of a transparent film can be determined from the relationship between the wavelength and focal length. This method has been highly successful in engineering measurements in recent years[166-170]. However, while these spectroscopic measurement methods are well-suited to thin transparent objects, they are unsuitable for thicker objects.

(a)

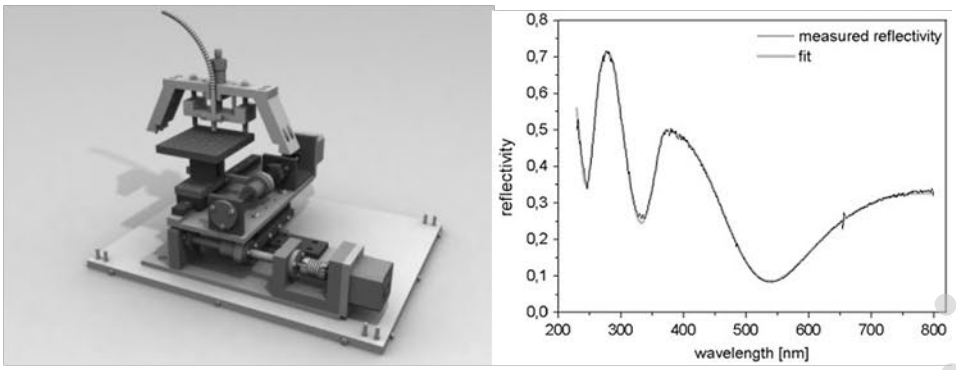

(b)

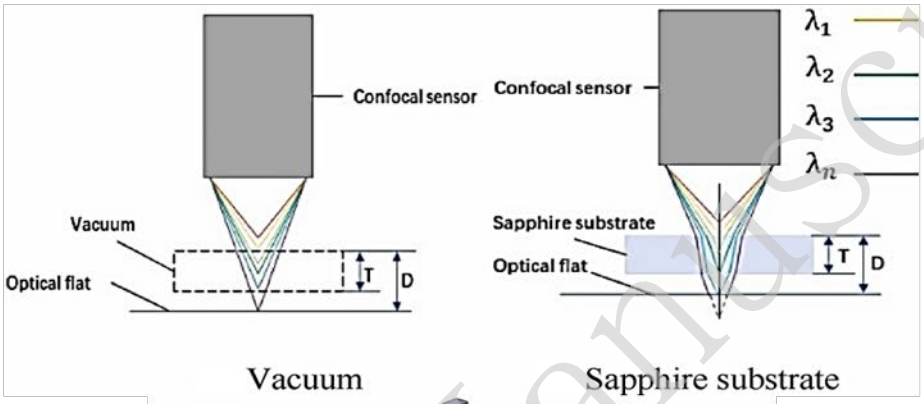

(c)

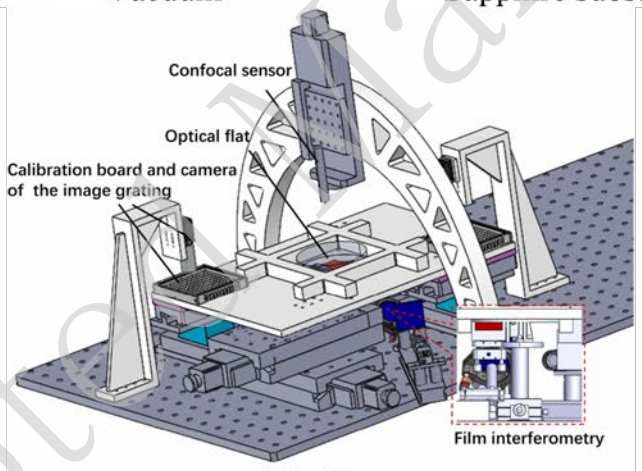

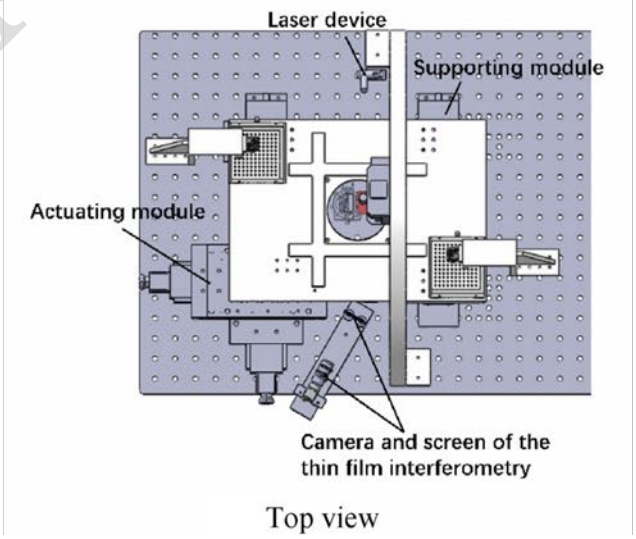

Figure 16. Spectroscopic and dispersion measurement methods. (a) Spectral reflectometry used for transparent film inspection, in which the left image depicts the system setup and the right image depicts the relationship between reflectivity and wavelength. The peaks and valleys of the curve can be interpreted to determine the thickness of the film at this position. Reproduced with permission[161]. Copyright 2004, John Wiley & Sons, Ltd. **(b)** and **(c)** Using a dispersion confocal sensor to inspect a transparent film, in which (b) depicts the principle of the dispersion confocal sensor and (c) depicts the system setup. Reproduced with permission[170]. Copyright 2023, Elsevier Inc.

General-scale Measurement Methods

General-scale measurement methods typically integrate various macro-scale and micro-scale measurement techniques to enhance measurement capabilities and address existing challenges in these respective measurement methodologies.

Low Transmittance Wavelength Methods

A wavelength with a low transmittance can be effectively employed to convert measurements of transparent objects into measurements of ordinary diffuse-reflecting objects. This is advantageous because non-destructive optical measurement methods for diffuse-reflecting objects are well-established and mature. As show in Fig.17, different materials exhibit varying spectral transmittance rates[171-173], the selection of suitable wavelengths can significantly enhance measurement efficiency. In this vein, Good et al. reported the transmittance rates of different transparent solar concentrators[174], and David et al. examined the transmittance rates of photovoltaic encapsulation materials[175]. These studies not only investigated the photoelectric properties of their subject materials but also detailed conditions for obtaining non-destructive measurements using low-transmittance wavelengths.

Several methods discussed above involve the use of low-transmittance wavelengths [40, 74, 89, 176, 177] to transform the complex problem of measuring transparent objects into a simpler problem of measuring diffused reflected objects; this facilitates the utilisation of various mature measurement techniques. Therefore, the use of low-transmittance wavelengths is advisable when addressing specific measurement problems because leveraging mature measurement methods can save time and resources.

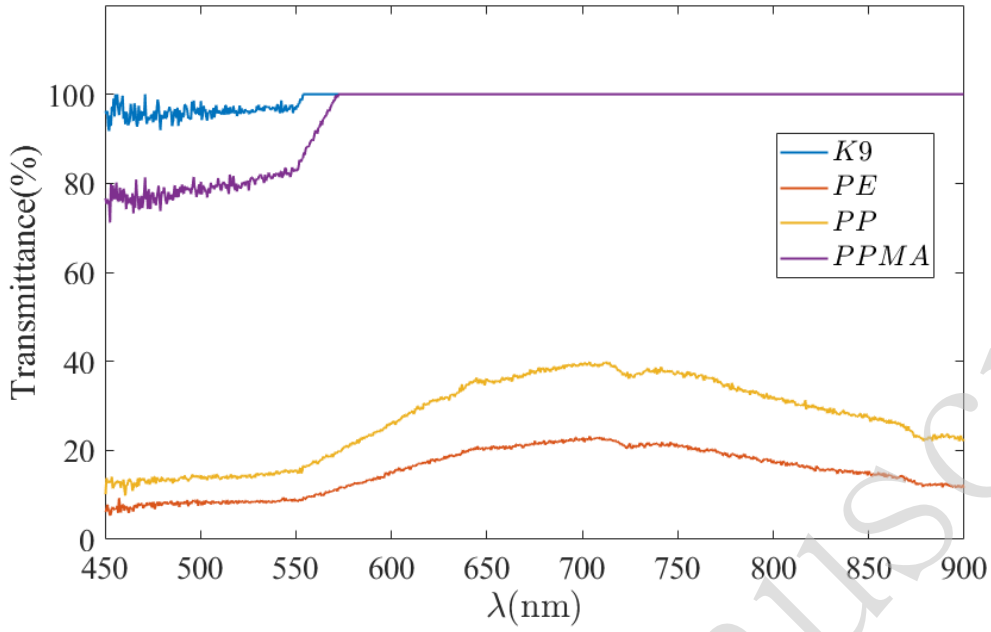

Figure 17. Transmittance spectrum of typical transparent materials measured by an FX2000 fibre spectrometer (ideaoptics, China) at room temperature. In the legend, K9 denotes an optical material (SiO_2 = 69.13%, B_2O_3 = 10.75%, BaO = 3.07%, Na_2O = 10.40%, K_2O = 6.29%, As_2O_3 = 0.36%) with a thickness of 1 mm, PE denotes polyethylene with a thickness of 3 mm, PP denotes polypropylene with a thickness of 1 mm, and PPMA denotes polymethyl methacrylate with a thickness of 2 mm.

Polarisation Measurement Methods

Polarisation represents another dimension of light that plays a critical role in various fields. The integration of polarisation information into other measurement methods can enhance the overall performance of the approach. Polarisation characteristics are commonly used to obtain the normal vectors of the surface microelements of an object or to determine the properties of the object directly; both approaches are described in the discussion of polarisation theory below. In addition, there have been many promising advances in the acquisition and processing of polarisation data; these advances are also described in this section.

Polarisation Measurement Theory

Transparent object measurement methods using polarisation can be generally divided into two categories: those that use polarisation to obtain normal surface vectors for reconstructing an object's three-dimensional structure and those that directly analyse

the relationship between the polarisation and surface properties of a material to extract the relevant information.

The normal vector can be obtained by describing the interaction of light with the surface of a transparent object using Fresnel's law, which establishes a close relationship between the direction of the normal surface vector and the polarisation characteristics of the outgoing light[178-180]. The existence of a unique relationship between the three-dimensional contour of a transparent surface and its normal vector allows the former to be reconstructed using the latter obtained from the polarisation information[181-184].

Wolff and Boult presented a theory on the polarisation properties of reflected light that respectively expresses the polarisation of specular reflected light and diffusely reflected light as follows[182]:

$$\rho_s = \frac{2\sin^2\theta_i \cos\theta_i \sqrt{n^2 - \sin^2\theta_i}}{n^2 - \sin^2\theta_i - n^2\sin^2\theta_i - 2\sin^4\theta_i} \tag{2}$$

$$\rho_d = \frac{\left(n - \frac{1}{n}\right)^2 \sin^2\theta_i}{2 + 2n^2 - \left(n + \frac{1}{n}\right)^2 \sin^2\theta_i + 4\cos\theta_i \sqrt{n^2 - \sin^2\theta_i}} \tag{3}$$

where n is the RI of the medium and θ_i is the incident angle of the light. Eq. 2 and Eq. 3 indicate that the polarisation of diffusely reflected light is monotonic with the incident angle, whereas the polarisation of specular reflected light is not. Thus, reconstructing an object using the polarisation of specular reflected light requires resolution of this ambiguity.

Researchers have proposed various solutions for addressing the angular ambiguity of normal vectors. Miyazaki et al. introduced a rotating target method[185, 186] that eliminates the need for a specific angle of rotation and avoids errors in system calibration; however, it requires multiple target measurements from different angles, which results in a complicated and time-consuming measurement process. In 2007, Miyazaki and Ikeuchi utilised the Mueller matrix to describe polarised light, thereby removing ambiguities while iteratively solving for the surface morphology[187].

Subsequently, multiple viewing angles have been employed to resolve ambiguity[178, 188], and the use of light-field cameras for rapid image acquisition with multiple viewing angles has been proposed[189-192].

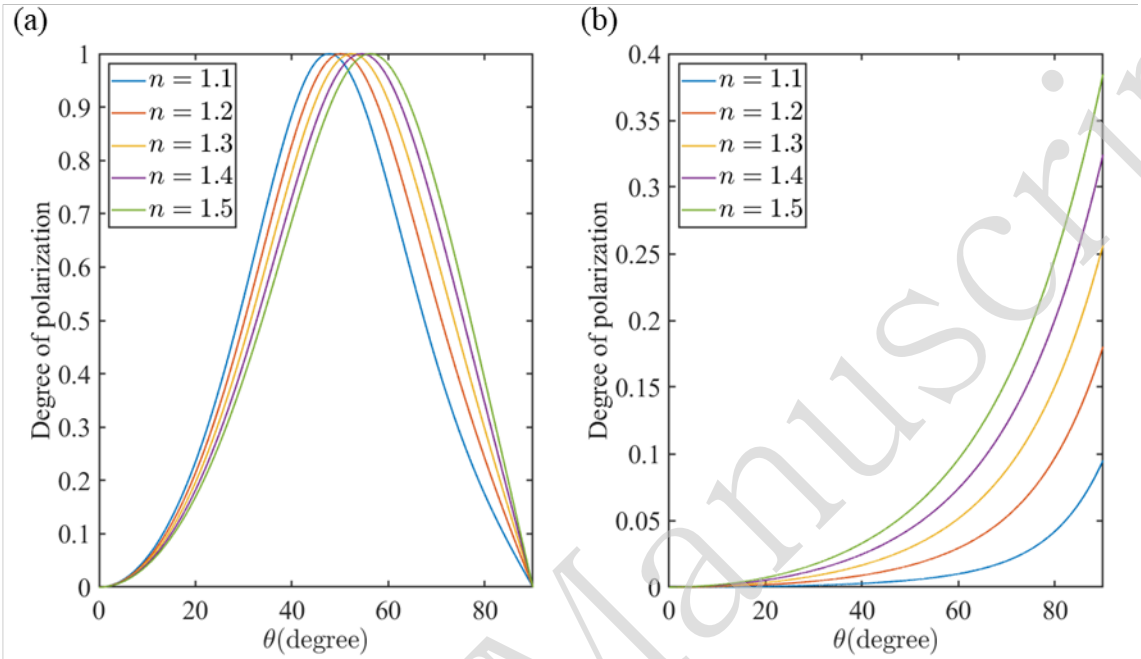

Figure 18. Relationship between incident angle and degree of polarisation according to RI for: (a) specular light and **(b)** diffused light.

The absence of angular ambiguity between diffuse light polarisation and the normal vector has led researchers to concentrate on separating out the diffused reflected light for three-dimensional reconstruction[179, 184, 190, 193-195]. However, the diffuse light reflected off a transparent object is weak, posing challenges for measuring its polarisation properties. Instead, the ambiguity of the normal vector can be addressed by leveraging the different RIs of various wavelengths of light, as shown in Fig. 18. Keikhosravi et al. achieved real-time detection of collagen fibres using multi-wavelength polarisation microscopy[196], which can also be combined with other acquisition methods to improve the measurement results[197, 198].

The use of Stokes vectors and Mueller matrices[183, 199] to describe polarisation represents an effective approach for the direct measurement of transparent objects based on their polarisation properties. Indeed, analysing the properties of the Stokes vectors and Mueller matrices to determine object polarisation properties is feasible. In 2019,

Wu et al. used Mueller matrices to distinguish between optical surface digs and dust by combining polarisation data with dark-field imaging[200], showcasing the potential of such dark-field polarisation systems for defect detection. Wei et al. used transmitted polarised structured light to classify and remove dust from optical devices, thereby mitigating its effects[201]. Moreover, haze, which comprises a multitude of dust, smoke and other dry particulates, is akin to the structures embedded in transparent objects and exhibits complex refraction and reflection phenomena. Liang et al. dehazed images using polarised light, realising a model that is potentially applicable to the inspection of transparent objects, particularly those with multiple microstructures, such as microbubbles[202, 203]. Ellipsometry is an effective tool for thin-film measurements and has been used to analyse the polarisation intensity in two orthogonal directions. Dual-wavelength[204] and multiple-wavelength[205-211] measurements have expanded the utility of ellipsometry. As the application of Stokes vectors and Mueller matrices to describe polarised light effectively utilises the information conveyed by light polarisation, further research on the use of Mueller matrices to capture multiple light refractions and reflections represents a promising direction for future research.

The polarisation properties of reflected and refracted light can also be analysed to characterise the properties of an object. In 2017, Kim and Ghosh used polarisation to measure the optical properties of transparent liquids[212], and Zhang et al. later employed circularly polarised light to measure the RI of metals[213]—a method that can be effectively adapted for use in transparent materials. In 2022, Fuentes-Domínguez et al. introduced a method for measuring nanostructures in transparent liquids by analysing the different acoustic responses of various nanostructures to differently polarised light; as shown in Fig. 19, this method can measure parameters such as shape, size, and position[214], and is anticipated to be applicable to the measurement of micro-scale or nano-scale defects in other transparent objects.

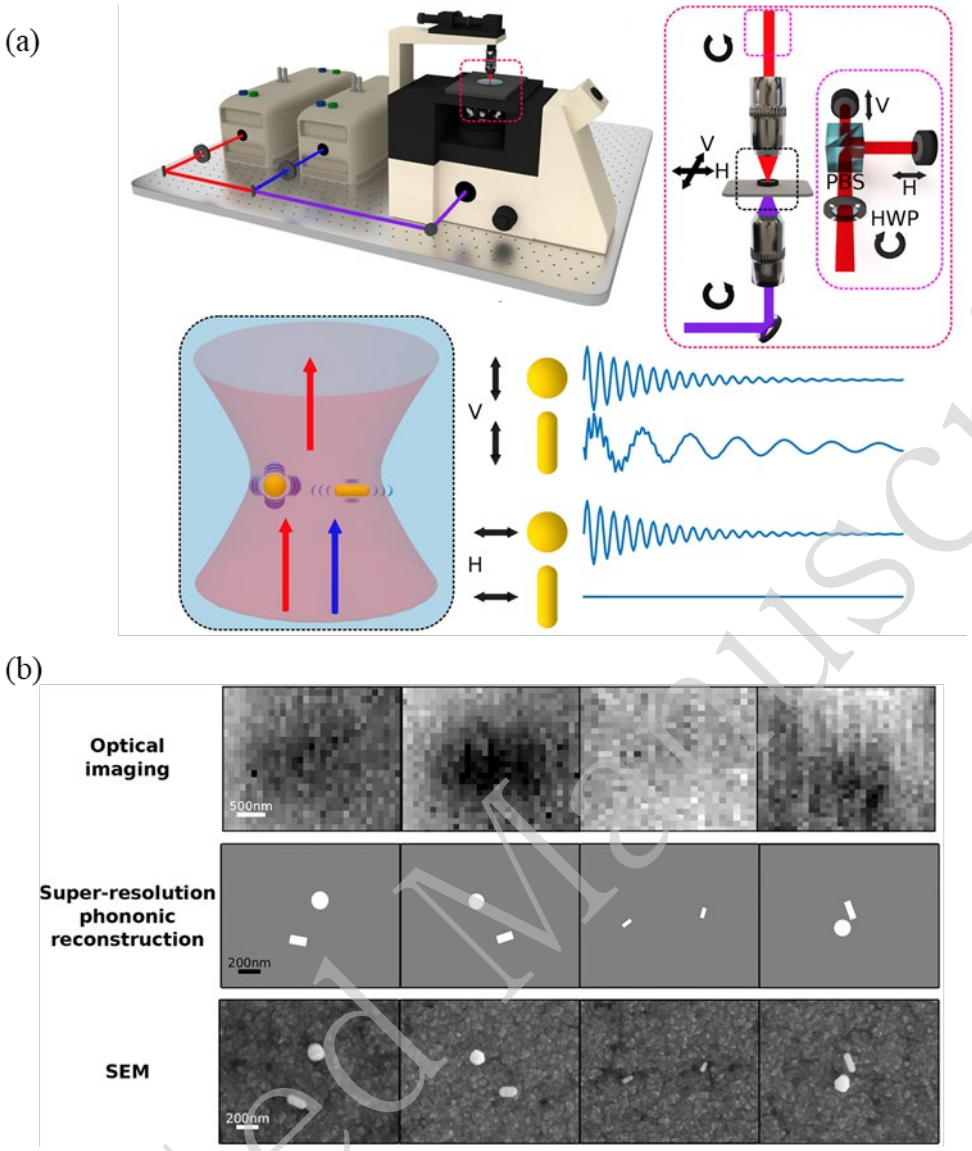

Figure 19. Reconstruction of nanostructures using polarised light. Reproduced with permission[214]. Copyright 2022, Creative Commons Attribution 4.0 International License. (a) System setup and acoustic responses of different nanostructures to differently polarised light. **(b)** Reconstruction results of different areas via super-resolution phononic reconstruction and scanning electron microscopy.

Furthermore, polarisation can be applied to enhance lower transmittance wavelengths, such as infrared or UV, and thereby improve inspection efficiency. This represents a special type of direct extrapolation that relies on polarisation properties. Kadambi et al. enhanced infrared time-of-flight measurement results using normal polarisation vectors[215, 216], and Liang et al. enhanced short-wave infrared images using visible light polarisation images[176]. The latter method considered the continuity of the image pixels to solve problems associated with the low resolution of infrared images;

this approach may be significant for the improvement of measurements at other wavelengths with low sensing resolutions.

Acquisition and Processing of Polarisation Images

Researchers have explored various methods for accelerating polarisation information acquisition speed and processing accuracy. One key challenge is dealing with the ambiguity of the specular reflected light, which requires obtaining four-angle maps. Traditional methods for doing so involve rotating the polariser; however, new approaches have emerged. Xin et al. accelerated the acquisition of multi-view and multi-angle polarisation images by fabricating adjustable polarisers and microlens arrays, known as twisted nematic liquid-crystal microlens arrays (TN-LCMLAs), using liquid crystals[191] (see Fig. 20 for details). Methods have also been developed for the acquisition of four-angle linear polarisation images in a single shot by incorporating etched four-quadrant micro-polarisers in front of camera pixel units[196, 217]. Furthermore, Rubin et al. designed a metasurface with a distributed birefringent medium to measure the full Stokes vector of light[218].

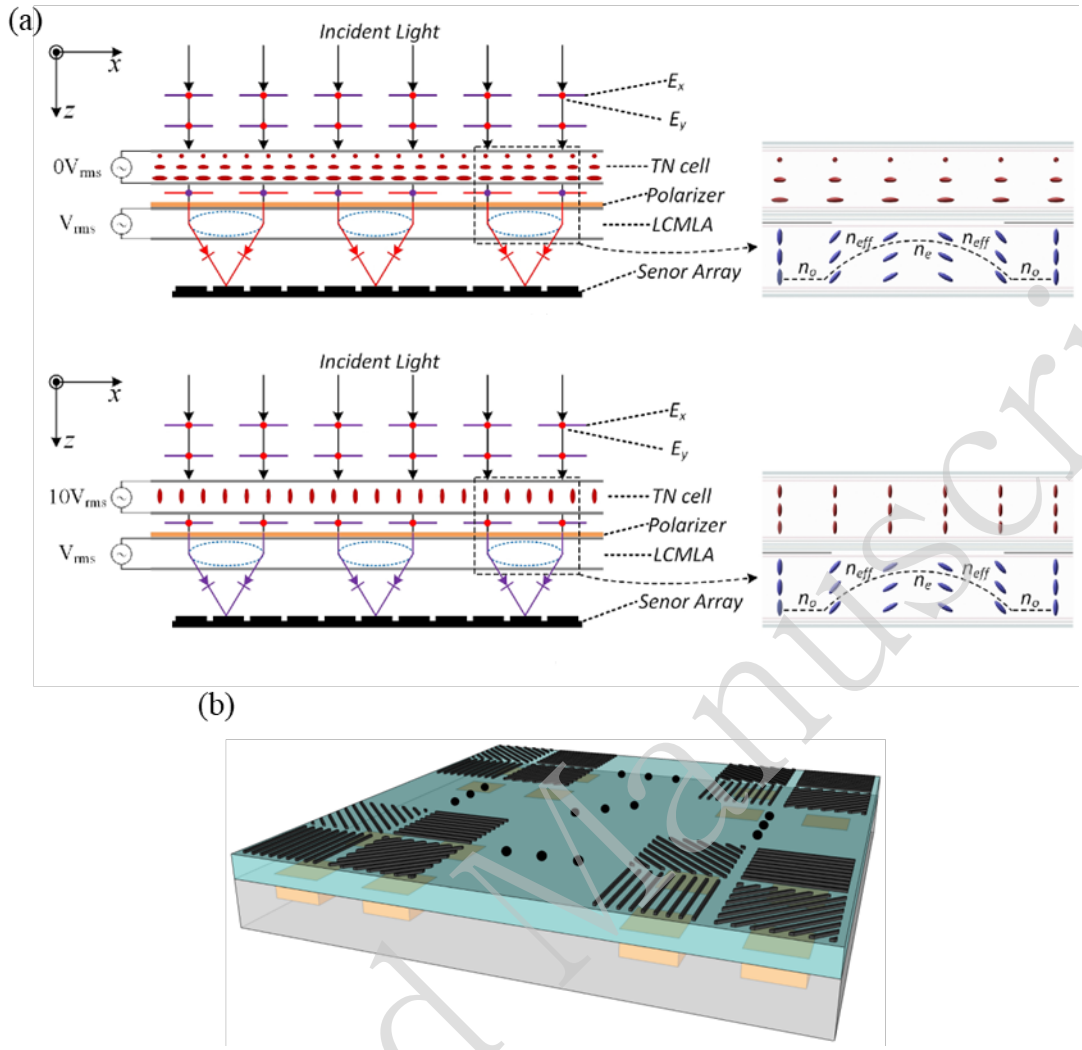

Figure 20. Special polarisation acquisition methods. (a) Structure of the TN-LCMLA, in which the upper structure is without external bias voltage and the polarisation state of the liquid crystal below changes when a bias voltage is provided. Reproduced with permission[191]. Copyright 2018, Optica Publishing Group. **(b)** Structure of the "super-pixel": four-quadrant micro-polariser in front of camera pixel units. Reproduced with permission[217]. Copyright 2015, Optica Publishing Group.

Recent advances in data processing capabilities have led to the integration of novel data processing and machine vision methods, such as deep learning and event cameras, with polarimetric measurement methods. Shao et al. applied deep learning to monocular image measurements of transparent objects by incorporating physics-based prior input images and prior confidence inputs based on Fresnel's law, thereby increasing the neural network credibility and reconstruction speed[219]. This approach demonstrates the potential of applying deep learning to reconstruct normal surface vectors using polarisation information. Furthermore, Muglikar et al. used a rotating line polariser and

event camera to address the trade-off between the lack of polarisation angle and time-consumption[220]. This idea can be applied to most methods that employ four-angle linear polarisation reconstruction to improve their accuracy without sacrificing inspection speed.

Discussion

This section clarifies the relationship between the measurement target and resolution requirements to assist readers in selecting an appropriate measurement method. Additionally, an analysis of the advantages and disadvantages associated with various methods is provided to facilitate effective evaluation of their strengths in different applications.

Measurement Target and Resolution Requirements

Various transparent object measurement methods were discussed in the previous sections. This section elucidates the relationship between the measurement target characteristics and resolution requirements to assist readers in selecting the appropriate measurement method. In addition, the advantages and disadvantages of the various methods are presented to facilitate their optimal application.

Resolution is a crucial consideration in any measurement task because different measurement targets require different levels of accuracy. Here, resolution refers to the ability to obtain the smallest true value, which is distinct from precision (a lower chance of error) and accuracy (a lower systematic error). Achieving a suitable resolution is vital because an insufficient resolution can make the measurement task challenging, whereas an excessive resolution can waste resources and reduce efficiency, especially in manufacturing applications. Several typical measurement types, their target transparent objects, and associated measurement requirements are described in this section.

Pose and position measurement: This type of measurement is widely required in robotics vision tasks, such as automated driving and industrial robotics, which often necessitate resolutions on the centimetre and millimetre scales. These applications

typically prioritise speed and efficiency over resolution owing to the need for a rapid response.

Defect measurement: This type of measurement includes the observation of surface and embedded defects and focuses on detection rather than dimensional measurement. Thus, the required resolution is determined according to the general scale of the defects.

Shape and surface geometry measurement: This is a common type of measurement that provides geometric parameters, such as surface profile and flatness. The required resolution depends on the application scenario; for example, measuring a general lens may require micron-level resolution, whereas measuring a reference mirror in an interferometer may require resolutions in the range of tens to hundreds of nanometres.

Three-dimensional structure measurement: This type of measurement captures the thickness of films, embedded structures, biological targets, etc. Film thickness measurement typically requires achieving the appropriate wavelength class (approximately one quarter or one half the wavelength of visible light), whereas biological measurements require only micron-scale resolution. Speed must also be considered in biological measurements because of phototoxicity and its effects on cellular activity.

Advantages and Disadvantages of Various Methods

Each non-destructive measurement method described in this review has its own scope of application, and the selection of an appropriate method considering its relevant advantages and disadvantages will ensure efficient and accurate measurements.

Macroscale measurement methods are suitable for centimetre- and millimetre-scale measurements, offering rapid but low-resolution results that are ideal for real-time applications. Machine vision is cost-effective but requires extensive computing resources. Structured light improves upon machine vision but has disadvantages such as the increased time cost and complexity associated with active light sources. Photothermal methods bypass light refraction and reflection but may cause

microstructural damage owing to excessive local temperature.

Micro-scale measurement methods target micron- and nanometre-scale measurements, often using interference methods to amplify differences. Traditional interference methods face challenges such as high coherent noise, environmental requirements, and cost. Digital holography offers high accuracy and wide application potential but has problems similar to those associated with traditional interferometry. Non-interference methods have low resolution and some uncertainty in their results but are widely applicable for small-scale measurements. Spectroscopy and dispersion methods are widely used for film inspection; however, they cannot yet measure thicker objects.

General-scale measurement methods can be combined with other methods to realise transferability but may not maximise the target's characteristics, leading to suboptimal results. Polarisation measurement methods offer the broadest possibilities when combined with other methods.

Thus, each method has its strengths and limitations, and the selection of the correct method depends on the specific measurement requirements and characteristics of the object being measured.

Table 1. Advantages and disadvantages of each method considered in this review.

Method	Measurement scale	Speed	Environmental limitations	Cost	Measurement target flexibility
Machine vision	Macro	+++	+/++	+	+++
Structured light	Macro	++	+	+	+++
Photothermal	Macro	+	+++	+++	+
Interference methods	Micro	++	+++	+++	+/++

Non-interference methods	Micro	+	++	+/++	+/++
Spectroscopy and dispersion	Micro	+	++	+++	+
Low transmitted wavelength	General	Depends on situation	+	+++	+++
Polarisation	General	Depends on situation	+	+	+++

Note: +, ++, and +++ represent the performance or demand in this field from lowest to highest.

Conclusion and Outlook

Methods for the non-destructive optical measurement of transparent objects are highly desirable. This review categorised these measurement methods according to their function on the macro-, micro-, and general scales. Several promising directions for the future development of such methods are outlined below based on the reviewed information.

Multi-method fusion: Combining multiple measurement methods represents a tremendously promising approach as individual measurement techniques often have specific limitations associated with trade-offs between measurement resolution and speed. However, industries such as semiconductor manufacturing require both high resolution and speed. The thoughtful fusion of measurement methods can compensate for the shortcomings of each individual method, thereby opening new possibilities for measurement.

Quantitative phase measurement techniques: Whether interferometric or non-interferometric, quantitative phase measurement techniques are well-suited to the measurement of transparent objects. Future progress in this field is expected with the ongoing development of new technologies.

Multiple data post-processing techniques: The rapid development of machine and deep learning methods has provided opportunities for improving data post-processing

capabilities. These methods can be used to improve both the measurement rate and resolution. Future research should focus on better utilising available computational data in such techniques.

Measurement and manufacturing are complementary processes, with advances in one driving progress in the other. Thus, the development of non-destructive technologies for measuring transparent objects will continue to expand in practical and industrial applications, promote the use of transparent components, and accelerate developments in optics and related fields.

Acknowledgements

This work was partially supported by the Shanghai Science and Technology Committee Innovation Grant (23ZR1404200) and National Natural Science Foundation of China (52075100, 52375414).

Conflict of interest

The authors declare no competing interests.

References

1. Morel, A. et al. Optical properties of the “clearest” natural waters. *Limnology and Oceanography* **52**, 217-229 (2007).
2. Westall, F. & Brack, A. The importance of water for life. *Space Science Reviews* **214**, 50 (2018).
3. Jacques, S. L. Optical properties of biological tissues: a review. *Physics in Medicine & Biology* **58**, R37-R61 (2013).
4. McClatchey, R. A. Optical Properties of the Atmosphere. 3rd edn. (Bedford: Air Force Cambridge Research Laboratories, 1972).
5. Rajaramakrishna, R. & Jakrapong, K. Glass material and their advanced applications. *KnE Social Sciences* **2019**, 796-807 (2019).
6. Geyer, R., Jambeck, J. R. & Law, K. L. Production, use, and fate of all plastics ever made. *Science Advances* **3**, e1700782 (2017).
7. Gibb, B. C. Plastics are forever. *Nature Chemistry* **11**, 394-395 (2019).
8. Hass, G. & Ritter, E. Optical film materials and their applications. *Journal of Vacuum Science and Technology* **4**, 71-79 (1967).
9. Wang, C. S. et al. Surface defect inspection and classification for glass screen of mobile phone. Proceedings of SPIE 11069, Tenth International Conference on Graphics and Image Processing (ICGIP 2018). Chengdu: SPIE, 2019, 110691U.

10. Yacoubian, A. Optical Systems and Components (CRC PRESS-TAYLOR & FRANCIS GROUP, 2015).

11. Cho, J. H., Cho, M. W. & Kim, M. K. Computer-aided design, manufacturing and inspection system integration for optical lens production. *International Journal of Production Research* **40**, 4271-4283 (2002).

12. Rebsamen, M., Boucheix, J. M. & Fayol, M. Quality control in the optical industry: from a work analysis of lens inspection to a training programme, an experimental case study. *Applied Ergonomics* **41**, 150-160 (2010).

13. Satorres Martínez, S. et al. A sensor planning system for automated headlamp lens inspection. *Expert Systems with Applications* **36**, 8768-8777 (2009).

14. Hideki, T. et al. Ultrahighly accurate 3D profilometer. Proceedings of SPIE 5638, Optical Design and Testing II. Beijing: SPIE, 2005.

15. Shenq-Tsong, C. et al. The measurement of optical and geometric parameters by a coordinate measuring machine. Proceedings of SPIE 8527, Multispectral, Hyperspectral, and Ultraspectral Remote Sensing Technology, Techniques and Applications IV. Kyoto: SPIE, 2012, 85270T.

16. Gigilashvili, D. et al. Translucency perception: a review. *Journal of Vision* **21**, 4 (2021).

17. Singh. M. Transparency and translucency. in Computer Vision: A Reference Guide (ed Ikeuchi, K.) (Cham: Springer, 2020), 1-5.

18. Burini Junior, E.C. et al. CIE 175:2006 A Framework for the Measurement of Visual Appearance. Proceedings of the CIE Expert Symposium on Visual Appearance. Paris: CIE 175, 2006.

19. Gupta, R. et al. Visibly transparent heaters. *ACS Applied Materials & Interfaces* **8**, 12559-12575 (2016).

20. Husain, A. A. F. et al. A review of transparent solar photovoltaic technologies. *Renewable and Sustainable Energy Reviews* **94**, 779-791 (2018).

21. Yu, H. L. et al. Semi-transparent organic photovoltaics. *Chemical Society Reviews* **52**, 4132-4148 (2023).

22. Zhu, H. L. et al. Transparent paper: fabrications, properties, and device applications. *Energy & Environmental Science* **7**, 269-287 (2014).

23. Jiang, J. Q. et al. Robotic perception of transparent objects: a review. *IEEE Transactions on Artificial Intelligence* **5**, 2547-2567 (2024).

24. Wang, S. F. et al. Transparent ceramics: processing, materials and applications. *Progress in Solid State Chemistry* **41**, 20-54 (2013).

25. McHenry, K., Ponce, J. & Forsyth, D. Finding glass. Proceedings of 2005 IEEE Computer Society Conference on Computer Vision and Pattern Recognition (CVPR 2005). San Diego: IEEE Computer Society, 2005, 973-979.

26. Xu, Y. C. et al. Light field distortion feature for transparent object classification. *Computer Vision and Image Understanding* **139**, 122-135 (2015).

27. Xu, Y. C. et al. TransCut2: transparent object segmentation from a light-field image. *IEEE Transactions on Computational Imaging* **5**, 465-477 (2019).

28. Tsai, D. et al. Distinguishing refracted features using light field cameras with application to structure from motion. *IEEE Robotics and Automation Letters* **4**, 177-184 (2019).

29. Zhou, Z. M. et al. GlassLoc: plenoptic grasp pose detection in transparent clutter. Proceedings of 2019 IEEE/RSJ International Conference on Intelligent Robots and Systems (IROS). Macau, China: IEEE, 2019, 4776-4783.

30. Tsai, D. et al. Refractive light-field features for curved transparent objects in structure from motion. *IEEE Robotics and Automation Letters* **6**, 6923-6930 (2021).

31. Wang, T., He, X. M. & Barnes, N. Glass object localization by joint inference of boundary and depth. Proceedings of the 21st International Conference on Pattern Recognition (ICPR2012). Tsukuba: IEEE, 2012, 3783-3786.

32. Madessa, A. H. et al. Leveraging an instance segmentation method for detection of transparent materials. Proceedings of 2019 IEEE SmartWorld, Ubiquitous Intelligence & Computing, Advanced & Trusted Computing, Scalable Computing & Communications, Cloud & Big Data Computing, Internet of People and Smart City Innovation (SmartWorld/SCALCOM/UIC/ATC/CBDCom/IOP/SCI). Leicester: IEEE, 2019, 406-412.

33. Xu, Z. G. et al. Real-time transparent object segmentation based on improved DeepLabv3+. Proceedings of 2021 China Automation Congress (CAC). Beijing: IEEE, 2021, 4310-4315.

34. Yu, L. T. et al. Progressive glass segmentation. *IEEE Transactions on Image Processing* **31**, 2920-2933 (2022).

35. Sajjan, S. et al. Clear grasp: 3D shape estimation of transparent objects for manipulation. Proceedings of 2020 IEEE International Conference on Robotics and Automation (ICRA). Paris: IEEE, 2020, 3634-3642.

36. Yu, H. X. et al. TGF-Net: Sim2Real transparent object 6D pose estimation based on geometric fusion. *IEEE Robotics and Automation Letters* **8**, 3868-3875 (2023).

37. Okada, K. et al. Whole shape estimation of transparent object from its contour using statistical shape model. Proceedings of 2023 IEEE/RSJ International Conference on Intelligent Robots and Systems (IROS). Detroit: IEEE, 2023, 1327-1333.

38. Kutulakos, K. N. & Steger, E. A theory of refractive and specular 3D shape by light-path triangulation. *International Journal of Computer Vision* **76**, 13-29 (2008).

39. Kim, J., Reshetouski, I. & Ghosh, A. Acquiring axially-symmetric transparent objects using single-view transmission imaging. Proceedings of 2017 IEEE Conference on Computer Vision and Pattern Recognition (CVPR). Honolulu: IEEE, 2017, 1484-1492.

40. Koyama, K. et al. 3D Shape Reconstruction of 3D Printed Transparent Microscopic Objects from Multiple Photographic Images Using Ultraviolet Illumination. *Micromachines* **9**, 261 (2018).

41. Gkioulekas, I., Levin, A. & Zickler, T. An evaluation of computational imaging techniques for heterogeneous inverse scattering. in Computer Vision – ECCV 2016 (eds Leibe, B. et al.) (Cham: Springer, 2016), 685-701.

42. Che, C. Q. et al. Towards learning-based inverse subsurface scattering. Proceedings of 2020 IEEE International Conference on Computational Photography (ICCP). St. Louis: IEEE, 2020, 1-12.

43. Martínez, S. S. et al. A machine vision system for defect characterization on transparent parts with non-plane surfaces. *Machine Vision and Applications* **23**, 1-13 (2012).

44. Martínez, S. S. et al. An industrial vision system for surface quality inspection of transparent parts. *The International Journal of Advanced Manufacturing Technology* **68**, 1123-1136 (2013).

45. Gruber, D. P. & Haselmann, M. Inspection of transparent objects with varying light scattering using a frangi filter. *Journal of Imaging* **7**, 27 (2021).

46. Gong, W. et al. Adaptive visual inspection method for transparent label defect detection of curved glass bottle. Proceedings of 2020 International Conference on Computer Vision, Image and Deep Learning (CVIDL). Chongqing: IEEE, 2020, 90-95.

47. Deng, Y. L., Xu, S. P. & Lai, W. W. A novel imaging-enhancement-based inspection method for transparent aesthetic defects in a polymeric polarizer. *Polymer Testing* **61**, 333-340 (2017).

48. Deng, Y. L. et al. Vison-based 3D shape measurement system for transparent microdefect characterization. *IEEE Access* **7**, 105721-105733 (2019).

49. Erozan, A. T., Bosse, S. & Tahoori, M. B. Defect detection in transparent printed electronics using learning-based optical inspection. *IEEE Transactions on Very Large Scale Integration (VLSI) Systems* **29**, 1505-1517 (2021).

50. Yin, Z. Y. et al. Efficient and precise detection for surface flaws on large-aperture optics based on machine vision and machine learning. *Optics & Laser Technology* **159**, 109011 (2023).

51. Taherimakhsousi, N. et al. Quantifying defects in thin films using machine vision. *npj Computational Materials* **6**, 111 (2020).

52. Farmahini-Farahani, M., Cheng, J. R. & Mosallaei, H. Metasurfaces nanoantennas for light processing. *Journal of the Optical Society of America B* **30**, 2365-2370 (2013).

53. Ruan, Z. C. et al. Spatial control of surface plasmon polariton excitation at planar metal surface. *Optics Letters* **39**, 3587-3590 (2014).

54. AbdollahRamezani, S. et al. Analog computing using graphene-based metalines. *Optics Letters* **40**, 5239-5242 (2015).

55. Pors, A., Nielsen, M. G. & Bozhevolnyi, S. I. Analog computing using reflective plasmonic metasurfaces. *Nano Letters* **15**, 791-797 (2015).

56. Chizari, A. et al. Analog optical computing based on a dielectric meta-reflect array. *Optics Letters* **41**, 3451-3454 (2016).

57. Lou, Y. J. et al. Spatial coupled-mode theory for surface plasmon polariton excitation at metallic gratings. *Journal of the Optical Society of America B* **33**, 819-824 (2016).

58. Cordaro, A. et al. High-index dielectric metasurfaces performing mathematical operations. *Nano Letters* **19**, 8418-8423 (2019).

59. Wan, L. et al. Optical analog computing of spatial differentiation and edge detection with dielectric metasurfaces. *Optics Letters* **45**, 2070-2073 (2020).

60. Xiao, T. T. et al. Realization of tunable edge-enhanced images based on computing metasurfaces. *Optics Letters* **47**, 925-928 (2022).

61. Li, Q. Y. et al. Surface topography detection based on an optical differential metasurface. *Optics Letters* **48**, 4801-4804 (2023).

62. Karimi, P., Khavasi, A. & Khaleghi, S. S. M. Fundamental limit for gain and resolution in analog optical edge detection. *Optics Express* **28**, 898-911 (2020).

63. Zhang, S. High-speed 3D shape measurement with structured light methods: a review. *Optics and Lasers in Engineering* **106**, 119-131 (2018).

64. Van der Jeught, S. & Dirckx, J. J. J. Real-time structured light profilometry: a review. *Optics and Lasers in Engineering* **87**, 18-31 (2016).

65. Xu, J. & Zhang, S. Status, challenges, and future perspectives of fringe projection profilometry. *Optics and Lasers in Engineering* **135**, 106193 (2020).

66. Geng, J. Structured-light 3D surface imaging: a tutorial. *Advances in Optics and Photonics* **3**, 128-160 (2011).

67. Huang, L. et al. Review of phase measuring deflectometry. *Optics and Lasers in Engineering* **107**, 247-257 (2018).

68. Ji, Y. J., Xia, Q. & Zhang, Z. J. Fusing depth and silhouette for scanning transparent object with RGB-D sensor. *International Journal of Optics* **2017**, 9796127 (2017).

69. Lei, H. & Asundi, A. A. Phase retrieval from reflective fringe patterns of double-sided transparent objects. *Measurement Science and Technology* **23**, 085201(2012).

70. Ye, J. Q. et al. In-situ deflectometic measurement of transparent optics in precision robotic polishing. *Precision Engineering* **64**, 63-69 (2020).

71. Yang, S. C. et al. Line-encoded structured light measurement method in measuring shiny and transparent objects. *Journal of Optics* **25**, 045701 (2023).

72. Liu, D., Chen, X. D. & Yang, Y. H. Frequency-based 3D reconstruction of transparent and specular objects. Proceedings of 2014 IEEE Conference on Computer Vision and Pattern Recognition. Columbus: IEEE, 2014, 660-667.

73. He, K. J. et al. 3D surface reconstruction of transparent objects using laser scanning with LTFtF method. *Optics and Lasers in Engineering* **148**, 106774 (2022).

74. Rantoson, R. et al. Non contact 3D measurement scheme for transparent objects using UV structured light. Proceedings of 2010 20th International Conference on Pattern Recognition. Istanbul: IEEE, 2010, 1646-1649.

75. Gu, J. W. et al. Compressive structured light for recovering inhomogeneous participating media. *IEEE Transactions on Pattern Analysis and Machine Intelligence* **35**, 1 (2013).
76. Huang, Y. Y. et al. Structured-light modulation analysis technique for contamination and defect detection of specular surfaces and transparent objects. *Optics Express* **27**, 37721-37735 (2019).
77. Guo, H. Y., Zhou, H. W. & Banerjee, P. P. Use of structured light in 3D reconstruction of transparent objects. *Applied Optics* **61**, B314-B324 (2022).
78. Trivedi, V. et al. Shape measurement of phase objects using fringe projection technique. Proceedings of SPIE 12618, Optical Measurement Systems for Industrial Inspection XIII. Munich: SPIE, 2023, 126182S.
79. Heredia Ortiz, M. E. Novel developments of Moiré techniques for industrial applications (University of Sheffield, 2004).
80. Xu, D. & Liechti, K. M. Bulge testing transparent thin films with moiré deflectometry. *Experimental Mechanics* **50**, 217-225 (2010).
81. Ri, S. & Muramatsu, T. A simple technique for measuring thickness distribution of transparent plates from a single image by using the sampling moiré method. *Measurement Science and Technology* **21**, 025305 (2010).
82. Thakur, M., Tay, C. J. & Quan, C. G. Surface profiling of a transparent object by use of phase-shifting Talbot interferometry. *Applied Optics* **44**, 2541-2545 (2005).
83. Meziane, R., Meguellati, S. & Messagier, M. Precision inspection of transparent component quality. *The International Journal of Advanced Manufacturing Technology* **125**, 1731-1741 (2023).
84. Bhattacharya, J. C. Measurement of the refractive index using the Talbot effect and a moire technique. *Applied Optics* **28**, 2600-2604(1989).
85. Samanta, K. & Joseph, J. An overview of structured illumination microscopy: recent advances and perspectives. *Journal of Optics* **23**, 123002 (2021).

86. Eren, G. et al. Scanning from heating: 3D shape estimation of transparent objects from local surface heating. *Optics Express* **17**, 11457-11468 (2009).
87. Mériaudeau, F. et al. “Scanning from heating” and “shape from fluorescence”: two non-conventional imaging systems for 3D digitization of transparent objects. in Depth Map and 3D Imaging Applications: Algorithms and Technologies (eds Malik, A. S. et al.) (Hershey: IGI Global, 2012), 229-243.
88. Meriaudeau, F. et al. 3-D scanning of nonopaque objects by means of imaging emitted structured infrared patterns. *IEEE Transactions on Instrumentation and Measurement* **59**, 2898-2906 (2010).
89. Gong, X. L. & Bansmer, S. 3-D ice shape measurements using mid-infrared laser scanning. *Optics Express* **23**, 4908-4926 (2015).
90. Brahm, A. et al. Non-destructive 3D shape measurement of transparent and black objects with thermal fringes. Proceedings of SPIE 9868, Dimensional Optical Metrology and Inspection for Practical Applications V. Baltimore: SPIE, 2016, 98680C.
91. Landmann, M. et al. High-resolution sequential thermal fringe projection technique for fast and accurate 3D shape measurement of transparent objects. *Applied Optics* **60**, 2362-2371 (2021).
92. Hlubina, P. Spectral reflectrometry and white-light interferometry used to measure thin films. Proceedings of SPIE 5457, Optical Metrology in Production Engineering. Strasbourg: SPIE, 2004, 756-764.
93. Sun, C. S. et al. Scanning white-light interferometer for measurement of the thickness of a transparent oil film on water. *Applied Optics* **44**, 5202-5205 (2005).
94. Li, M. C., Wan, D. S. & Lee, C. C. Application of white-light scanning interferometer on transparent thin-film measurement. *Applied Optics* **51**, 8579-8586 (2012).
95. Leong-Hoï, A. et al. Detection of defects in a transparent polymer with high resolution tomography using white light scanning interferometry and

noise reduction. Proceedings of SPIE 9528, Videometrics, Range Imaging, and Applications XIII. Munich: SPIE, 2015, 952807.

96. Kühnhold, P. et al. Transparent layer thickness measurement using low-coherence interference microscopy. Proceedings of SPIE 9525, Optical Measurement Systems for Industrial Inspection IX. Munich: SPIE, 2015, 95252F.

97. Hwang, C. H. et al. Inspection of laser ablated transparent conductive oxide thin films by a multifunction optical measurement system. in Emerging Challenges for Experimental Mechanics in Energy and Environmental Applications, Proceedings of the 5th International Symposium on Experimental Mechanics and 9th Symposium on Optics in Industry (ISEM-SOI), 2015 (eds Martínez-García, A. et al.) (Cham: Springer, 2017), 173-179.

98. Guo, T. et al. Surface measurement through transparent medium using Linnik type white-light spectral interferometer. Proceedings of SPIE 10827, Sixth International Conference on Optical and Photonic Engineering (icOPEN 2018). Shanghai: SPIE, 2018, 1082705.

99. Bulun, G. et al. Construction of a time-domain full-field OCT for non-contact volumetric layer thickness measurement. Proceedings of SPIE 12618, Optical Measurement Systems for Industrial Inspection XIII. Munich: SPIE, 2013, 126180S.

100. Guo, T. et al. Surface measurement through transparent medium using Linnik type white-light spectral interferometer. Proceedings of SPIE 10872, Sixth International Conference on Optical and Photonic Engineering (icOPEN 2018). Shanghai: SPIE, 2018, 1082705.

101. Schnars, U. & Jüptner, W. Direct recording of holograms by a CCD target and numerical reconstruction. *Applied Optics* **33**, 179-181 (1994).

102. Kreis, T. in Handbook of Holographic Interferometry 35-219 (Wiley-VCH, 2004).

103. Kebbel, V., Hartmann, H. J. & Jueptner, W. P. O. Application of digital holographic microscopy for inspection of micro-optical components.

Proceedings of SPIE 4398, Optical Measurement Systems for Industrial Inspection II: Application in Industrial Design. Munich: SPIE, 2001, 189-198.

104. Kim, M. K. Digital Holographic Microscopy: Principles, Techniques, and Applications. (New York: Springer, 2011), 149-190.

105. Osten, W. et al. Recent advances in digital holography [Invited]. *Applied Optics* **53**, G44-G63 (2014).

106. Tahara, T. et al. Digital holography and its multidimensional imaging applications: a review. *Microscopy* **67**, 55-67 (2018).

107. Cuche, E., Bevilacqua, F. & Depeursinge, C. Digital holography for quantitative phase-contrast imaging. *Optics Letters* **24**, 291-293 (1999).

108. Kemper, B. & von Bally, G. Digital holographic microscopy for live cell applications and technical inspection. *Applied Optics* **47**, A52-A61 (2008).

109. Kemper, B. et al. Characterisation of light emitting diodes (LEDs) for application in digital holographic microscopy for inspection of micro and nanostructured surfaces. *Optics and Lasers in Engineering* **46**, 499-507 (2008).

110. Picart, P., Mounier, D. & Desse, J. M. High-resolution digital two-color holographic metrology. *Optics Letters* **33**, 276-278 (2008).

111. Gabai, H. & Shaked, N. T. Dual-channel low-coherence interferometry and its application to quantitative phase imaging of fingerprints. *Optics Express* **20**, 26906-26912 (2012).

112. Min, J. W. et al. Optical thickness measurement with single-shot dual-wavelength in-line digital holography. *Optics Letters* **43**, 4469-4472 (2018).

113. Kühn, J. et al. Axial sub-nanometer accuracy in digital holographic microscopy. *Measurement Science and Technology* **19**, 074007 (2008).

114. Turko, N. A. & Shaked, N. T. Simultaneous two-wavelength phase unwrapping using an external module for multiplexing off-axis holography. *Optics Letters* **42**, 73-76 (2017).

115. Li, X. et al. Dual-wavelength real-time simultaneous phase imaging based on off-axis interferometry. *Optics and Lasers in Engineering* **165**, 107565 (2023).

116. Mark, A. S. et al. Semiconductor wafer defect detection using digital holography. Proceedings of SPIE 5041, Process and Materials Characterization and Diagnostics in IC Manufacturing. Santa Clara: SPIE, 2003.

117. Tayebi, B. et al. Transparent stepped phase measurement using two illuminating beams. Proceedings of SPIE 9203, Interferometry XVII: Techniques and Analysis. San Diego: SPIE, 2014, 920306.

118. Qu, W. J. et al. Transmission digital holographic microscopy based on a beam-splitter cube interferometer. *Applied Optics* **48**, 2778-2783 (2009).

119. Ebrahimi, S. et al. Stable and simple quantitative phase-contrast imaging by Fresnel biprism. *Applied Physics Letters* **112**, 113701 (2018).

120. Sun, T. F. et al. Quantitative phase imaging using dual-channel Fresnel bi-prism interference microscope. Proceedings of SPIE 10964, Tenth International Conference on Information Optics and Photonics. Beijing: SPIE, 2018, 109640T.

121. Monemhaghdoust, Z. et al. Dual wavelength full field imaging in low coherence digital holographic microscopy. *Optics Express* **19**, 24005-24022 (2011).

122. Rostykus, M. & Moser, C. Compact lensless off-axis transmission digital holographic microscope. *Optics Express* **25**, 16652-16659 (2017).

123. Chhaniwal, V. et al. Quantitative phase-contrast imaging with compact digital holographic microscope employing Lloyd's mirror. *Optics Letters* **37**, 5127-5129 (2012).

124. Andrushchak, A. S. et al. Interferometric technique for controlling wedge angle and surface flatness of optical slabs. *Optics and Lasers in Engineering* **51**, 342-347 (2013).

125. Zhang, J. W. et al. A review of common-path off-axis digital holography: towards high stable optical instrument manufacturing. *Light: Advanced Manufacturing* **2**, 23 (2021).

126. Singh, A. S. G. et al. Lateral shearing digital holographic imaging of small biological specimens. *Optics Express* **20**, 23617-23622 (2012).

127. Seo, K. B., Kim, B. M. & Kim, E. S. Digital holographic microscopy based on a modified lateral shearing interferometer for three-dimensional visual inspection of nanoscale defects on transparent objects. *Nanoscale Research Letters* **9**, 471 (2014).

128. Di, J. L. et al. Dual-wavelength common-path digital holographic microscopy for quantitative phase imaging based on lateral shearing interferometry. *Applied Optics* **55**, 7287-7293 (2016).

129. Di, J. L. et al. Quantitative and dynamic phase imaging of biological cells by the use of the digital holographic microscopy based on a beam displacer unit. *IEEE Photonics Journal* **10**, 1-10 (2018).

130. Sun, T. F. et al. Michelson-based lateral shearing interference microscopy for quantitative phase measurement of biological cells. *Japanese Journal of Applied Physics* **59**, 106504 (2020).

131. Sun, T. F. et al. Single-shot interference microscopy using a wedged glass plate for quantitative phase imaging of biological cells. *Laser Physics* **28**, 125601 (2018).

132. Anand, A. et al. Single beam Fourier transform digital holographic quantitative phase microscopy. *Applied Physics Letters* **104**, 103705 (2014).

133. Li, Z. D. et al. Optical measurement of photonic nanostructures based on quantitative phase microscopy. 2023 Photonics & Electromagnetics Research Symposium (PIERS). Prague: IEEE, 2023, 643-648.

134. Mahajan, S. et al. Highly stable digital holographic microscope using Sagnac interferometer. *Optics Letters* **40**, 3743-3746 (2015).

135. Jafarfard, M. R. et al. Dual-wavelength diffraction phase microscopy for simultaneous measurement of refractive index and thickness. *Optics Letters* **39**, 2908-2911 (2014).

136. Besaga, V. R. et al. Digital holographic microscopy for sub-μm scale high aspect ratio structures in transparent materials. *Optics and Lasers in Engineering* **121**, 441-447 (2019).

137. Xia, H. T. et al. Non-invasive mechanical measurement for transparent objects by digital holographic interferometry based on iterative least-squares phase unwrapping. *Experimental Mechanics* **52**, 439-445 (2012).

138. Madsen, A. E. G. et al. On-axis digital holographic microscopy: Current trends and algorithms. *Optics Communications* **537**, 129458 (2023).

139. Zuo, C. et al. Transport of intensity equation: a tutorial. *Optics and Lasers in Engineering* **135**, 106187 (2020).

140. Zheng, G. A., Horstmeyer, R. & Yang, C. H. E. Wide-field, high-resolution Fourier ptychographic microscopy. *Nature Photonics* **7**, 739-745 (2013).

141. Gerchberg, R. W. & Saxton, W. O. Phase determination from image and diffraction plane pictures in the electrom microscope. *Optik* (*International Journal for Light and Electron Optics*) **34**, 275-284 (1971).

142. Gerchberg, R. W. & Saxton, W. O. A practical algorithm for the determination of phase from image and diffraction plane pictures. *Optik* (*International Journal for Light and Electron Optics*) **35**, 237-246 (1972).

143. Fienup, J. R. Phase retrieval algorithms: a comparison. *Applied Optics* **21**, 2758-2769 (1982).

144. Teague, M. R. Deterministic phase retrieval: a Green's function solution. *Journal of the Optical Society of America* **73**, 1434-1441 (1983).

145. Zuo, C. et al. Transport of intensity phase retrieval and computational imaging for partially coherent fields: the phase space perspective. *Optics and Lasers in Engineering* **71**, 20-32 (2015).

146. Barty, A. et al. Quantitative phase tomography. *Optics Communications* **175**, 329-336 (2000).

147. Roberts, A. et al. Refractive-index profiling of optical fibers with axial symmetry by use of quantitative phase microscopy. *Optics Letters* **27**, 2061-2063 (2002).

148. Ampem-Lassen, E. et al. Refractive index profiling of axially symmetric optical fibers: a new technique. *Optics Express* **13**, 3277-3282 (2005).

149. Kou, S. S. et al. Transport-of-intensity approach to differential interference contrast (TI-DIC) microscopy for quantitative phase imaging. *Optics Letters* **35**, 447-449 (2010).

150. Waller, L. et al. Transport of intensity phase imaging in a volume holographic microscope. *Optics Letters* **35**, 2961-2963 (2010).

151. Zuo, C. et al. High-speed transport-of-intensity phase microscopy with an electrically tunable lens. *Optics Express* **21**, 24060-24075 (2013).

152. Zuo, C. et al. Noninterferometric single-shot quantitative phase microscopy. *Optics Letters* **38**, 3538-3541 (2013).

153. Zuo, C. et al. Boundary-artifact-free phase retrieval with the transport of intensity equation II: applications to microlens characterization. *Optics Express* **22**, 18310-18324 (2014).

154. Nguyen, T. et al. Fully automated, high speed, tomographic phase object reconstruction using the transport of intensity equation in transmission and reflection configurations. *Applied Optics* **54**, 10443-10453 (2015).

155. Zuo, C. et al. Lensless phase microscopy and diffraction tomography with multi-angle and multi-wavelength illuminations using a LED matrix. *Optics Express* **23**, 14314-14328 (2015).

156. Li, J. J. et al. Transport of intensity diffraction tomography with non-interferometric synthetic aperture for three-dimensional label-free microscopy. *Light: Science & Applications* **11**, 154 (2022).

157. Li, P. et al. Separation of three-dimensional scattering effects in tilt-series Fourier ptychography. *Ultramicroscopy* **158**, 1-7 (2015).

158. Horstmeyer, R. et al. Diffraction tomography with Fourier ptychography. *Optica* **3**, 827-835 (2016).

159. Zuo, C. et al. Wide-field high-resolution 3D microscopy with Fourier ptychographic diffraction tomography. *Optics and Lasers in Engineering* **128**, 106003 (2020).

160. Tian, L. & Waller, L. 3D intensity and phase imaging from light field measurements in an LED array microscope. *Optica* **2**, 104-111 (2015).

161. Urbánek, M. et al. Instrument for thin film diagnostics by UV spectroscopic reflectometry. *Surface and Interface Analysis* **36**, 1102-1105 (2004).

162. Nečas, D. et al. Assessment of non-uniform thin films using spectroscopic ellipsometry and imaging spectroscopic reflectometry. *Thin Solid Films* **571**, 573-578 (2014).

163. Ohlídal, I. et al. Combination of spectroscopic ellipsometry and spectroscopic reflectometry with including light scattering in the optical characterization of randomly rough silicon surfaces covered by native oxide layers. *Surface Topography: Metrology and Properties* **7**, 045004 (2019).

164. Bahrenberg, L. et al. Characterization of nanoscale gratings by spectroscopic reflectometry in the extreme ultraviolet with a stand-alone setup. *Optics Express* **28**, 20489-20502 (2020).

165. Joo, K.-N. & Park, H.-M. Recent Progress on Optical Tomographic Technology for Measurements and Inspections of Film Structures. *Micromachines* **13**, 1074 (2022).

166. Miks, A., Novak, J. & Novak, P. Analysis of method for measuring thickness of plane-parallel plates and lenses using chromatic confocal sensor. *Applied Optics* **49**, 3259-3264 (2010).

167. Hillenbrand, M. et al. Parallelized chromatic confocal sensor systems. Proceedings of SPIE 8788, Optical Measurement Systems for Industrial Inspection VIII. Munich: SPIE, 2013, 87880V.

168. Fu, S. W. et al. In-situ measurement of surface roughness using chromatic confocal sensor. *Procedia CIRP* **94**, 780-784 (2020).

169. Bai, J. et al. A new method to measure spectral reflectance and film thickness using a modified chromatic confocal sensor. *Optics and Lasers in Engineering* **154**, 107019 (2022).

170. Cheng, F. et al. A double-sided surface scanning platform for sapphire substrate quality assessment. *Precision Engineering* **84**, 191-201 (2023).

171. Wakaki, M. et al. Physical Properties and Data of Optical Materials (Boca Raton: CRC Press, 2017), 576.

172. McCarthy, D. E. Transmittance of optical materials from 0.17 *μ* to 3.0 *μ*. *Applied Optics* **6**, 1896-1898 (1967).

173. Gillespie, D. T., Olsen, A. L. & Nichols, L. W. Transmittance of optical materials at high temperatures in the 1-*μ* to 12-*μ* range. *Applied Optics* **4**, 1488-1493 (1965).

174. Good, P. et al. Spectral reflectance, transmittance, and angular scattering of materials for solar concentrators. *Solar Energy Materials and Solar Cells* **144**, 509-522 (2016).

175. Miller, D. C. et al. Examination of an optical transmittance test for photovoltaic encapsulation materials. Proceedings of SPIE 8825, Reliability of Photovoltaic Cells, Modules, Components, and Systems VI. San Diego: SPIE, 2013, 882509.

176. Liang, J. et al. High-resolution reconstruction of shortwave infrared polarimetric images using the intensity information of visible images. *Applied Optics* **58**, 4866-4870 (2019).

177. Liang, J. et al. Short-wave infrared polarimetric image reconstruction using a deep convolutional neural network based on a high-frequency correlation. *Applied Optics* **61**, 7163-7172 (2022).

178. Miyazaki, D. et al. Surface normal estimation of black specular objects from multiview polarization images. *Optical Engineering* **56**, 041303 (2016).

179. Atkinson, G. A. & Hancock, E. R. Recovery of surface orientation from diffuse polarization. *IEEE Transactions on Image Processing* **15**, 1653-1664 (2006).

180. Wolff, L. B. Polarization vision: a new sensory approach to image understanding. *Image and Vision Computing* **15**, 81-93 (1997).

181. Wolff, L.B. & Boult, T.E. in Physics-Based Vision: Principles and Practice (eds. Wolff, L.B., Shafer, S.A. & Healey, G.E.) 424 (A K Peters/CRC Press, New York, 1993).

182. Wolff, L. B. & Boult, T. E. Constraining object features using a polarization reflectance model. *IEEE Transactions on Pattern Analysis and Machine Intelligence* **13**, 635-657 (1991).

183. Petrov, N. I. & Porfirev, A. P. Special issue on polarized light and optical systems. *Photonics* **9**, 570 (2022).

184. Sato, Y., Wheeler, M. D. & Ikeuchi, K. Object shape and reflectance modeling from observation. Proceedings of the 24th Annual Conference on Computer Graphics and Interactive Techniques. New York: ACM Press, 1997, 379-387.

185. Miyazaki, D., Kagesawa, M. & Ikeuchi, K. Determining shapes of transparent objects from two polarization images. Proceedings of the IAPR Conference on Machine Vision Applications. Nara: Japan, 2002, 26-31.

186. Miyazaki, D., Kagesawa, M. & Ikeuchi, K. Transparent surface modeling from a pair of polarization images. *IEEE Transactions on Pattern Analysis and Machine Intelligence* **26**, 73-82 (2004).

187. Miyazaki, D. & Ikeuchi, K. Shape estimation of transparent objects by using inverse polarization ray tracing. *IEEE Transactions on Pattern Analysis and Machine Intelligence* **29**, 2018-2030 (2007).

188. Ping, X. X. et al. 3-D reconstruction of textureless and high-reflective target by polarization and binocular stereo vision. *Journal of Infrared and Millimeter Waves* **36**, 432-438 (2017).

189. Oldenbourg, R. Polarized light field microscopy: an analytical method using a microlens array to simultaneously capture both conoscopic and orthoscopic views of birefringent objects. *Journal of Microscopy* **231**, 419-32 (2008).

190. Kim, J. & Ghosh, A. Polarized light field imaging for single-shot reflectance separation. *Sensors* **18**, 3803 (2018).

191. Xin, Z. W. et al. Dual-polarized light-field imaging micro-system via a liquid-crystal microlens array for direct three-dimensional observation. *Optics Express* **26**, 4035-4049 (2018).

192. Tran, M. T. & Oldenbourg, R. Point spread function of the polarized light field microscope. *Journal of the Optical Society of America A* **39**, 1095-1103 (2022).

193. Klasing, K. et al. Comparison of surface normal estimation methods for range sensing applications. Proceedings of 2009 IEEE International Conference on Robotics and Automation. Kobe: IEEE, 2009, 3206-3211.

194. Ma, F. Y. et al. Single-shot 3D reconstruction imaging approach based on polarization properties of reflection lights. Proceedings of SPIE 11898, Holography, Diffractive Optics, and Applications XI. Nantong: SPIE, 2021, 118980F.

195. Han, P. L. et al. Computational polarization 3D: new solution for monocular shape recovery in natural conditions. *Optics and Lasers in Engineering* **151**, 106925 (2022).

196. Keikhosravi, A. et al. Real-time polarization microscopy of fibrillar collagen in histopathology. *Scientific Reports* **11**, 19063 (2021).

197. Zhao, J. Y., Monno, Y. & Okutomi, M. Polarimetric multi-view inverse rendering. *IEEE Transactions on Pattern Analysis and Machine Intelligence* **45**, 8798-8812 (2023).

198. Hao, J. L. et al. 3D reconstruction of high-reflective and textureless targets based on multispectral polarization and machine vision. *Acta Geodaetica et Cartographica Sinica* **47**, 816-824 (2018).

199. Ren, L. Y. et al. Polarimetric optical imaging: devices, technologies and applications (invited). *Acta Photonica Sinica* **51**, 0851505 (2022).

200. Wu, F. et al. Classification between digs and dust particles on optical surfaces with acquisition and analysis of polarization characteristics. *Applied Optics* **58**, 1073-1083 (2019).

201. Wei, W. et al. Surface defect detection in transparent objects using polarized transmission structured light. *Acta Optica Sinica* **41**, 1812002 (2021).

202. Liang, J., Ren, L. Y. & Liang, R. G. Low-pass filtering based polarimetric dehazing method for dense haze removal. *Opt Express* **29**, 28178-28189 (2021).

203. Liang, J. et al. Polarimetric dehazing method for dense haze removal based on distribution analysis of angle of polarization. *Optics Express* **23**, 26146-26157(2015).

204. Kim, Y. N. et al. Device based in-chip critical dimension and overlay metrology. *Optics Express* **17**, 21336-21343 (2009).

205. Mendoza-Galván, A. et al. Mueller matrix spectroscopic ellipsometry study of chiral nanocrystalline cellulose films. *Journal of Optics* **20**, 024001 (2018).

206. Ngo, D. et al. Spectroscopic ellipsometry study of thickness and porosity of the alteration layer formed on international simple glass surface in aqueous corrosion conditions. *npj Materials Degradation* **2**, 20 (2018).

207. Thomas, E. L. H. et al. Spectroscopic ellipsometry of nanocrystalline diamond film growth. *ACS Omega* **2**, 6715-6727 (2017).

208. Hajduk, B., Bednarski, H. & Trzebicka, B. Temperature-dependent spectroscopic ellipsometry of thin polymer films. *The Journal of Physical Chemistry B* **24**, 3229-3251 (2020).

209. Yoo, S. & Park, Q. H. Spectroscopic ellipsometry for low-dimensional materials and heterostructures. *Nanophotonics* **11**, 15 (2022).

210. Lee, S. W. et al. Co-axial spectroscopic snap-shot ellipsometry for real-time thickness measurements with a small spot size. *Optics Express* **28**, 25879-25893 (2020).

211. Richter, S. et al. Broadband femtosecond spectroscopic ellipsometry. *Review of Scientific Instruments* **92**, 033104 (2021).

212. Kim, J. & Ghosh, A. Practical acquisition of translucent liquids using polarized transmission imaging. ACM SIGGRAPH 2017 Posters. Los Angeles: ACM, 2017, 84.

213. Zhang, Y. et al. Refractive index inversion method for metals based on circular polarization detection of light. *Optics Communications* **535**, 129344 (2023).

214. Fuentes-Domínguez, R. et al. Polarization-sensitive super-resolution phononic reconstruction of nanostructures. *ACS Photonics* **9**, 1919-1925 (2022).

215. Kadambi, A. et al. Polarized 3D: synthesis of polarization and depth cues for enhanced 3D sensing. SIGGRAPH 2015: Studio. Los Angeles: ACM, 2015, 23.

216. Kadambi, A. et al. Polarized 3D: high-quality depth sensing with polarization cues. Proceedings of 2015 IEEE International Conference on Computer Vision (ICCV). Santiago: IEEE, 2015, 3370-3378.

217. Garcia, N. M. et al. Surface normal reconstruction using circularly polarized light. *Opt Express* **23**, 14391-406 (2015).

218. Rubin, N. A. et al. Matrix Fourier optics enables a compact full-Stokes polarization camera. *Science* **365**, 43 (2019).

219. Shao, M. Q. et al. Transparent shape from a single view polarization image. 2023 IEEE/CVF International Conference on Computer Vision (ICCV). Paris: IEEE, 2023, 9243-9252.

220. Muglikar, M. et al. Event-based shape from polarization. Proceedings of 2023 IEEE/CVF Conference on Computer Vision and Pattern Recognition. Vancouver: IEEE, 2023, 1547-1556.